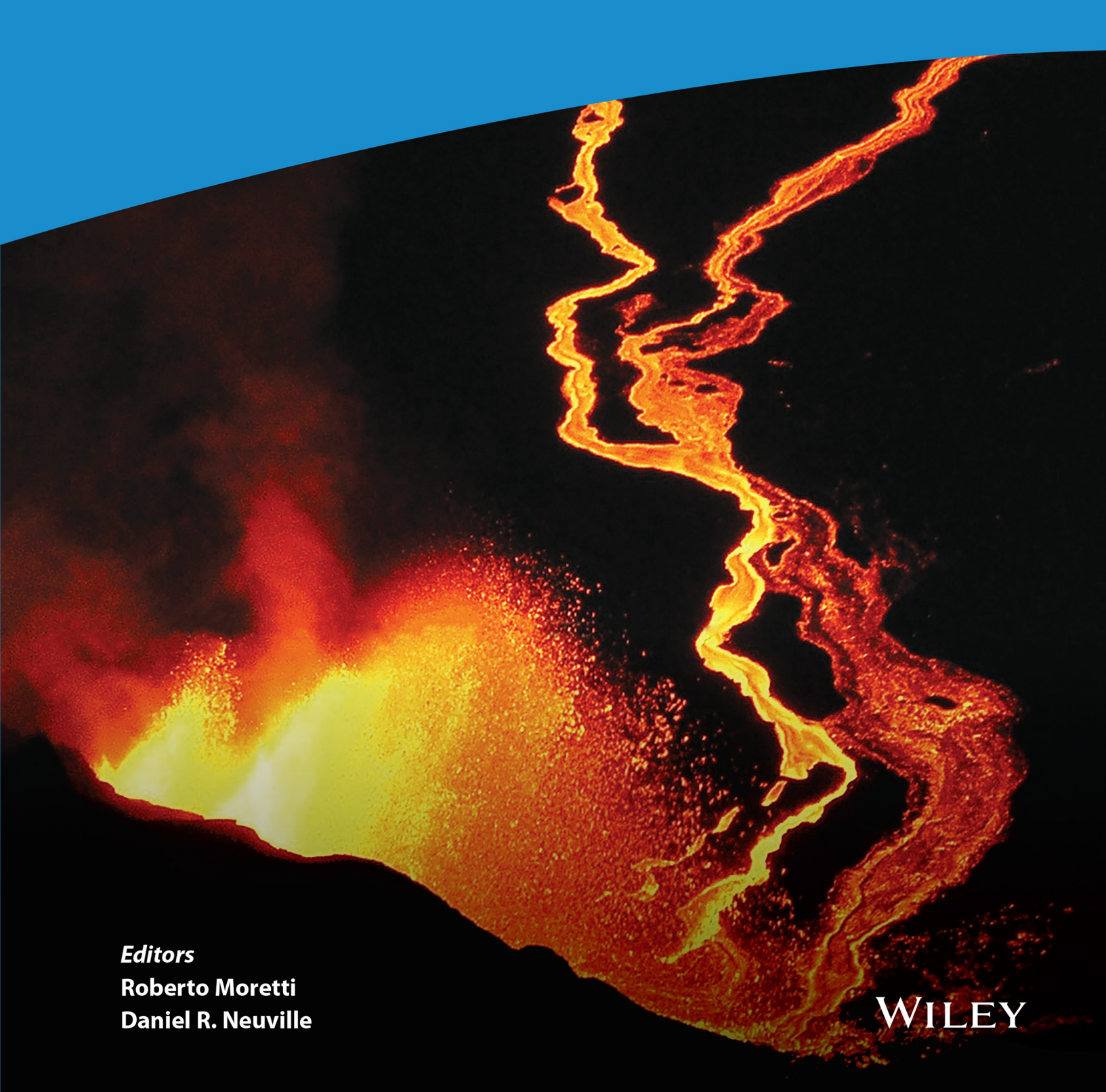
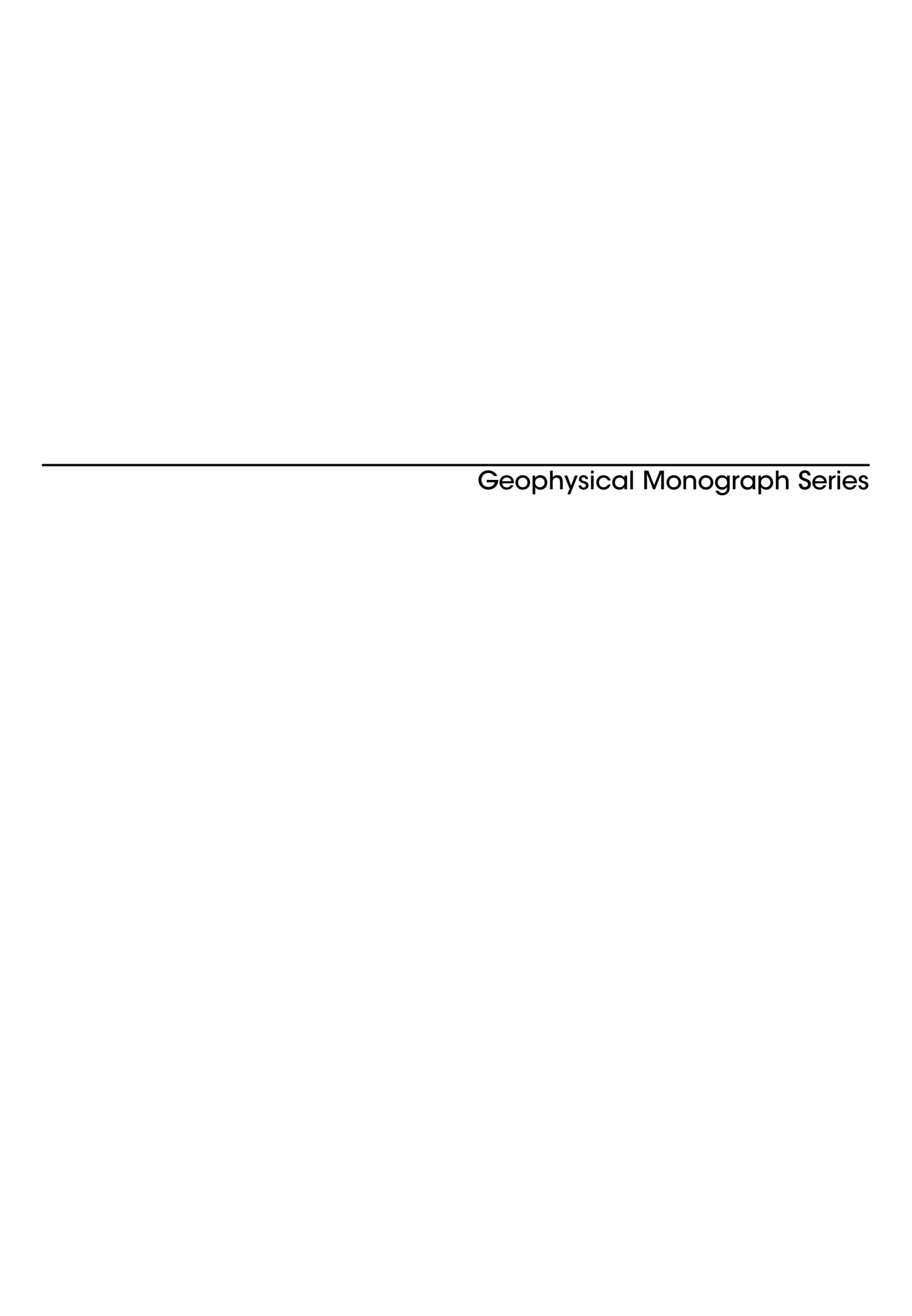


Magma Redox Geochemistry





- 217 Deep Earth: Physics and Chemistry of the Lower Mantle and Core Hidenori Terasaki and Rebecca A. Fischer (Eds.)
- 218 Integrated Imaging of the Earth: Theory and Applications
 Max Moorkamp, Peter G. Lelievre, Niklas Linde, and Amir
 Khan (Eds.)
- **219 Plate Boundaries and Natural Hazards** *Joao Duarte and Wouter Schellart (Eds.)*
- 220 Ionospheric Space Weather: Longitude and Hemispheric Dependences and Lower Atmosphere Forcing Timothy Fuller-Rowell, Endawoke Yizengaw, Patricia H. Doherty, and Sunanda Basu (Eds.)
- 221 Terrestrial Water Cycle and Climate Change Natural and Human-Induced Impacts Qiuhong Tang and Taikan Oki (Eds.)
- **222** Magnetosphere-lonosphere Coupling in the Solar System Charles R. Chappell, Robert W. Schunk, Peter M. Banks, James L. Burch, and Richard M. Thorne (Eds.)
- 223 Natural Hazard Uncertainty Assessment: Modeling and Decision Support Karin Riley, Peter Webley, and Matthew Thompson (Eds.)
- 224 Hydrodynamics of Time-Periodic Groundwater Flow:
 Diffusion Waves in Porous Media Joe S. Depner and Todd C.
 Rasmussen (Auth.)
- **225** Active Global Seismology Ibrahim Cemen and Yucel Yilmaz (Eds.)
- **226** Climate Extremes Simon Wang (Ed.)
- **227 Fault Zone Dynamic Processes** *Marion Thomas (Ed.)*
- 228 Flood Damage Survey and Assessment: New Insights from Research and Practice Daniela Molinari, Scira Menoni, and Francesco Ballio (Eds.)
- **229** Water-Energy-Food Nexus Principles and Practices *P. Abdul Salam, Sangam Shrestha, Vishnu Prasad Pandey, and Anil K Anal (Eds.)*
- **230** Dawn–Dusk Asymmetries in Planetary Plasma Environments
 Stein Haaland, Andrei Rounov, and Colin Forsyth (Eds.)
- **231 Bioenergy and Land Use Change** Zhangcai Qin, Umakant Mishra, and Astley Hastings (Eds.)
- 232 Microstructural Geochronology: Planetary Records Down to Atom Scale Desmond Moser, Fernando Corfu, James Darling, Steven Reddy, and Kimberly Tait (Eds.)
- 233 Global Flood Hazard: Applications in Modeling, Mapping and Forecasting Guy Schumann, Paul D. Bates, Giuseppe T. Aronica, and Heiko Apel (Eds.)
- 234 Pre-Earthquake Processes: A Multidisciplinary Approach to Earthquake Prediction Studies Dimitar Ouzounov, Sergey Pulinets, Katsumi Hattori, and Patrick Taylor (Eds.)
- 235 Electric Currents in Geospace and Beyond Andreas Keiling, Octav Marghitu, and Michael Wheatland (Eds.)
- **236 Quantifying Uncertainty in Subsurface Systems** Celine Scheidt, Lewis Li, and Jef Caers (Eds.)
- 237 Petroleum Engineering Moshood Sanni (Ed.)
- 238 Geological Carbon Storage: Subsurface Seals and Caprock Integrity Stephanie Vialle, Jonathan Ajo-Franklin, and J. William Carey (Eds.)
- **239 Lithospheric Discontinuities** Huaiyu Yuan and Barbara Romanowicz (Eds.)
- **240 Chemostratigraphy Across Major Chronological Eras** *Alcides N.Sial, Claudio Gaucher, Muthuvairavasamy Ramkumar, and Valderez Pinto Ferreira (Eds.)*
- 241 Mathematical Geoenergy:Discovery, Depletion, and Renewal Paul Pukite, Dennis Coyne, and Daniel Challou (Eds.)

- **242 Ore Deposits: Origin, Exploration, and Exploitation** *Sophie Decree and Laurence Robb (Eds.)*
- 243 Kuroshio Current: Physical, Biogeochemical and Ecosystem Dynamics Takeyoshi Nagai, Hiroaki Saito, Koji Suzuki, and Motomitsu Takahashi (Eds.)
- **244** Geomagnetically Induced Currents from the Sun to the Power Grid Jennifer L. Gannon, Andrei Swidinsky, and Zhonghua Xu (Eds.)
- **245 Shale: Subsurface Science and Engineering** *Thomas Dewers, Jason Heath, and Marcelo Sánchez (Eds.)*
- 246 Submarine Landslides: Subaqueous Mass Transport Deposits From Outcrops to Seismic Profiles Kei Ogata, Andrea Festa, and Gian Andrea Pini (Eds.)
- 247 Iceland: Tectonics, Volcanics, and Glacial Features Tamie J. Jovanelly
- **248 Dayside Magnetosphere Interactions** *Qiugang Zong, Philippe Escoubet, David Sibeck, Guan Le, and Hui Zhang (Eds.)*
- **249** Carbon in Earth's Interior Craig E. Manning, Jung-Fu Lin, and Wendy L. Mao (Eds.)
- 250 Nitrogen Overload: Environmental Degradation, Ramifications, and Economic Costs Brian G. Katz
- 251 Biogeochemical Cycles: Ecological Drivers and Environmental Impact Katerina Dontsova, Zsuzsanna Balogh-Brunstad, and Gaël Le Roux (Eds.)
- 252 Seismoelectric Exploration: Theory, Experiments, and Applications Niels Grobbe, André Revil, Zhenya Zhu, and Evert Slob (Eds.)
- **253 El Niño Southern Oscillation in a Changing Climate** *Michael J. McPhaden, Agus Santoso, and Wenju Cai (Eds.)*
- 254 Dynamic Magma Evolution Francesco Vetere (Ed.)
- 255 Large Igneous Provinces: A Driver of Global Environmental and Biotic Changes Richard. E. Ernst, Alexander J. Dickson, and Andrey Bekker (Eds.)
- 256 Coastal Ecosystems in Transition: A Comparative Analysis of the Northern Adriatic and Chesapeake Bay Thomas C.

 Malone, Alenka Malei, and Jadran Faganeli (Eds.)
- 257 Hydrogeology, Chemical Weathering, and Soil Formation Allen Hunt, Markus Egli, and Boris Faybishenko (Eds.)
- **258 Solar Physics and Solar Wind** *Nour E. Raouafi and Angelos Vourlidas (Eds.)*
- 259 Magnetospheres in the Solar System Romain Maggiolo, Nicolas André, Hiroshi Hasegawa, and Daniel T. Welling (Eds.)
- **260 Ionosphere Dynamics and Applications** *Chaosong Huang and Gang Lu (Eds.)*
- **261 Upper Atmosphere Dynamics and Energetics** *Wenbin Wang and Yongliang Zhang (Eds.)*
- **262 Space Weather Effects and Applications** *Anthea J. Coster, Philip J. Erickson, and Louis J. Lanzerotti (Eds.)*
- **263 Mantle Convection and Surface Expressions** Hauke Marquardt, Maxim Ballmer, Sanne Cottaar, and Jasper Konter (Eds.)
- **264** Crustal Magmatic System Evolution: Anatomy, Architecture, and Physico-Chemical Processes Matteo Masotta, Christoph Beier, and Silvio Mollo (Eds.)
- 265 Global Drought and Flood Observation, Modeling, and Prediction Huan Wu, Dennis P. Lettenmaier, Qiuhong Tang, and Philip J. Ward (Eds.)
- **Magma Redox Geochemistry** Roberto Moretti and Daniel R. Neuville (Eds.)

Magma Redox Geochemistry

Roberto Moretti Daniel R. Neuville Editors

This Work is a co-publication of the American Geophysical Union and John Wiley and Sons, Inc.



WILEY

This edition first published 2022 © 2022 American Geophysical Union

All rights reserved. No part of this publication may be reproduced, stored in a retrieval system, or transmitted, in any form or by any means, electronic, mechanical, photocopying, recording or otherwise, except as permitted by law. Advice on how to obtain permission to reuse material from this title is available at http://www.wiley.com/go/permissions.

The right of Roberto Moretti and Daniel R. Neuville to be identified as the editor of this work has been asserted in accordance with law.

Published under the aegis of the AGU Publications Committee

Matthew Giampoala, Vice President, Publications Carol Frost, Chair, Publications Committee For details about the American Geophysical Union visit us at www.agu.org.

Registered Office

John Wiley & Sons, Inc., 111 River Street, Hoboken, NJ 07030, USA

Editorial Office

111 River Street, Hoboken, NJ 07030, USA

For details of our global editorial offices, customer services, and more information about Wiley products visit us at www.wiley.com.

Wiley also publishes its books in a variety of electronic formats and by print-on-demand. Some content that appears in standard print versions of this book may not be available in other formats.

Limit of Liability/Disclaimer of Warranty

While the publisher and authors have used their best efforts in preparing this work, they make no representations or warranties with respect to the accuracy or completeness of the contents of this work and specifically disclaim all warranties, including without limitation any implied warranties of merchantability or fitness for a particular purpose. No warranty may be created or extended by sales representatives, written sales materials or promotional statements for this work. The fact that an organization, website, or product is referred to in this work as a citation and/or potential source of further information does not mean that the publisher and authors endorse the information or services the organization, website, or product may provide or recommendations it may make. This work is sold with the understanding that the publisher is not engaged in rendering professional services. The advice and strategies contained herein may not be suitable for your situation. You should consult with a specialist where appropriate. Further, readers should be aware that websites listed in this work may have changed or disappeared between when this work was written and when it is read. Neither the publisher nor authors shall be liable for any loss of profit or any other commercial damages, including but not limited to special, incidental, consequential, or other damages.

Library of Congress Cataloging-in-Publication Data

Names: Moretti, Roberto, editor. | Neuville, Daniel R., editor.

Title: Magma redox geochemistry / Roberto Moretti, Daniel R. Neuville, editors.

Description: Hoboken, NJ: Wiley-American Geophysical Union, [2022] |

Series: Geophysical monograph series | Includes index.

Identifiers: LCCN 2021027133 (print) | LCCN 2021027134 (ebook) | ISBN

9781119473251 (cloth) | ISBN 9781119473299 (adobe pdf) | ISBN

9781119473244 (epub)

Subjects: LCSH: Oxidation-reduction reaction. | Magmas.

Classification: LCC QD63.O9 M34 2021 (print) | LCC QD63.O9 (ebook) | DDC

541/.393-dc23

LC record available at https://lccn.loc.gov/2021027133

LC ebook record available at https://lccn.loc.gov/2021027134

Cover Design: Wiley

Cover Image: Lava fountaining and lava flows emitted from a fissure that opened in the wall of the Enclos Fouqué caldera at Piton de la Fournaise on December 27, 2005; © Aline Peltier (IPGP/OVPF)

Set in 10/12pt Times New Roman by Straive, Pondicherry, India

CONTENTS

List	of Contributors	vi
Pref	ace	ix
1	Redox Equilibria: From Basic Concepts to the Magmatic Realm	1
Part	I: Redox from the Earth's Accretion to Global Geodynamics	19
2	Redox Processes Before, During, and After Earth's Accretion Affecting the Deep Carbon Cycle Vincenzo Stagno and Sonja Aulbach	21
3	Oxygen Fugacity Across Tectonic Settings	33
4	Redox Variables and Mechanisms in Subduction Magmatism and Volcanism	63
5	Redox Melting in the Mantle	93
Part	II: Redox at Work: From Magma Sources to Volcanic Phenomena	115
6	Ionic Syntax and Equilibrium Approach to Redox Exchanges in Melts: Basic Concepts and the Case of Iron and Sulfur in Degassing Magmas	117
7	The Petrological Consequences of the Estimated Oxidation State of Primitive MORB Glass	139
8	Oxygen Content, Oxygen Fugacity, the Oxidation State of Iron, and Mid-Ocean Ridge Basalts	155
9	Chromium Redox Systematics in Basaltic Liquids and Olivine	165
10	The Thermodynamic Controls on Sulfide Saturation in Silicate Melts with Application to Ocean Floor Basalts	177
11	Redox State of Volatiles and Their Relationships with Iron in Silicate Melts: Implications for Magma Degassing	215

12	Iron in Silicate Glasses and Melts: Implications for Volcanological Processes	233
Part	III: Tools and Techniques to Characterize the Redox and its Effect on Isotope Partitioning	255
13	How to Measure the Oxidation State of Multivalent Elements in Minerals, Glasses, and Melts? Daniel R. Neuville, Maria Rita Cicconi, and Charles Le Losq	257
14	Oxidation State, Coordination, and Covalency Controls on Iron Isotopic Fractionation in Earth's Mantle and Crust: Insights from First-Principles Calculations and NRIXS Spectroscopy Marc Blanchard and Nicolas Dauphas	283
15	The Role of Redox Processes in Determining the Iron Isotope Compositions of Minerals, Melts, and Fluids Paolo A. Sossi and Baptiste Debret	303
16	Zinc and Copper Isotopes as Tracers of Redox Processes	331
17	Mineral-Melt Partitioning of Redox-Sensitive Elements Guilherme Mallmann, Antony D. Burnham, and Raul O.C. Fonseca	345
18	Titanomagnetite – Silicate Melt Oxybarometry	369
19	The Redox Behavior of Rare Earth Elements Maria Rita Cicconi, Charles Le Losq, Grant S. Henderson, and Daniel R. Neuville	381
Inde	x	399

LIST OF CONTRIBUTORS

Róbert Arató

Bayerisches Geoinstitut University of Bayreuth Bayreuth, Germany

Paul D. Asimow

Division of Geological and Planetary Sciences California Institute of Technology Pasadena, CA, USA

Andreas Audétat

Bayerisches Geoinstitut University of Bayreuth Bayreuth, Germany

Sonja Aulbach

Institute of Geosciences Goethe-Universität Frankfurt am Main, Germany

Aaron S. Bell

Department of Geological Sciences University of Colorado Boulder Boulder, CO, USA

Andrew J. Berry

Research School of Earth Sciences Australian National University Canberra, ACT, Australia

Suzanne K. Birner

Division of Natural Sciences, Nursing, and Mathematics Berea College Berea, KY, USA

Marc Blanchard

Géosciences Environnement Toulouse (GET) Université de Toulouse CNRS, IRD Toulouse, France

Maryjo Brounce

Department of Earth and Planetary Sciences University of California Riverside Riverside, CA, USA

Antony D. Burnham

Research School of Earth Sciences Australian National University Canberra, ACT, Australia

Maria Rita Cicconi

Université de Paris Institut de Physique du Globe de Paris Paris, France; and

Department of Materials Science and Engineering Friedrich-Alexander-Universität Erlangen-Nürnberg Erlangen, Germany

Elizabeth Cottrell

Department of Mineral Sciences National Museum of Natural History Smithsonian Institution Washington, DC, USA

Nicolas Dauphas

Origins Laboratory
Department of the Geophysical Sciences
and Enrico Fermi Institute
The University of Chicago
Chicago, IL, USA

Fred A. Davis

Department of Earth and Environmental Sciences University of Minnesota Duluth Duluth, MN, USA

Baptiste Debret

Université de Paris Institut de Physique du Globe de Paris Paris, France; and Laboratoire G-Time DGES Université Libre de Bruxelles Brussels, Belgium

Katy A. Evans

School of Earth and Planetary Sciences Curtin University Perth, Western Australia, Australia

Stephen F. Foley

Department of Earth and Environmental Sciences, and ARC Centre of Excellence for Core to Crust Fluid Systems Macquarie University Sydney, New South Wales, Australia

Raul O.C. Fonseca

Institute of Geology, Mineralogy and Geophysics Ruhr-University Bochum Bochum, Germany

Grant S. Henderson

Department of Earth Sciences University of Toronto Toronto, Canada

Edward C. Inglis

Université de Paris Institut de Physique du Globe de Paris Paris, France

Katherine A. Kelley

Graduate School of Oceanography University of Rhode Island Narragansett, RI, USA

Charles Le Losq

Research School of Earth Sciences Australian National University Canberra, ACT, Australia; and Université de Paris Institut de Physique du Globe de Paris Paris, France

Guilherme Mallmann

Research School of Earth Sciences Australian National University Canberra, ACT, Australia

Nicole Métrich

Université de Paris Institut de Physique du Globe de Paris Paris, France

Roberto Moretti

Université de Paris Institut de Physique du Globe de Paris Paris, France

Frédéric Moynier

Université de Paris Institut de Physique du Globe de Paris Paris, France

Daniel R. Neuville

Université de Paris Institut de Physique du Globe de Paris Paris, France

Hugh St.C. O'Neill

Research School of Earth Sciences Australian National University Canberra, ACT, Australia

Paolo A. Sossi

Institute of Geochemistry and Petrology ETH Zürich Zürich, Switzerland; and Université de Paris Institut de Physique du Globe de Paris Paris, France

Vincenzo Stagno

Department of Earth Sciences Sapienza University of Rome Rome, Italy

Andy G. Tomkins

School of Earth, Atmosphere and Environment Monash University Melbourne, Victoria, Australia

Laura E. Waters

Department of Earth and Environmental Science New Mexico Institute of Mining and Technology Socorro, NM, USA

PREFACE

In chemistry, redox issues occupy a central role for our understanding of how chemical exchanges take place between substances. Redox reactions include all chemical reactions in which atoms have their oxidation state changed because of the transfer of electrons between chemical species. Such a transfer involves both a reduction process and a complementary oxidation process and the consequent rearranging of chemical bonds.

The word oxidation originally implied reaction with oxygen to form an oxide, since dioxygen (O₂) was historically the first recognized oxidizing agent. Later, the term was expanded to encompass oxygen-like substances that accomplished parallel chemical reactions. Ultimately, the meaning was generalized to include all processes involving loss of electrons. The word reduction originally referred to the loss in weight upon heating a metallic ore, such as a metal oxide to extract the metal. In other words, ore was "reduced" to metal. Antoine Lavoisier (1743-1794) showed that this loss of weight was due to the loss of oxygen as a gas. This etymological premise also summarizes the significance that for a long time the world of geology has been attributed to the concept of "redox." In high-temperature geology, where aqueous solutions can no more be defined, redox has an upmost importance to both the formation of minerals and the mobilization of metals. However, it is often intended as a measure of oxygen fugacity (fO_2), anchored to an assemblage of minerals or compounds which constrains its variations as a simple function of temperature.

The redox state is one of the master variables driving Earth-forming processes and since the dawn of geochemistry, knowledge of redox state has been essential to understanding the compositional makeup of our planet and the fundamental processes occurring from the core up to the atmosphere. Most of these processes involve the major transport agent of matter on Earth, i.e., magma. The social and economic impact of redox geochemistry is enormous, because of the control played on metal mobility, solubility, and availability by redox state of metals and ligands that may complex them, and because of the widespread use of redox indicators for environmental hazards assessment, such as the volcanic one, which assessment greatly benefits from studies on volcanic gas speciation, which in turn is controlled by redox. Volatile components and their redox control on volcanic degassing and metal mobility offer good examples of redox exchanges in high-temperature environments close to human experience. Knowledge of redox mechanisms acting in volcanism and hydrothermalism have a great impact on the socioeconomic development of human societies because of their key role in volcanic hazard assessment, geothermal energy exploration, and ore deposits formation.

As shown in this monograph, redox state is also an image of the magma composition, and the understanding of magma (particularly melt) physicochemical nature is the basic prerequisite to understand how redox exchanges work in deep Earth systems and to understand "who controls what." The latter is a difficult task, given the almost infinite conditions of temperature, pressure, and chemical composition relevant to igneous petrology. However, the study of redox state and related properties cannot be reduced to simple rule of thumbs or assumptions such as the existence of stoichiometric mineral assemblages buffering oxygen fugacity via solid-gas equilibria.

Knowledge of the redox potential (or alternatively, oxygen fugacity) at which a rock forms and evolves is relevant for interpreting the rock's history. However, the approach inherited by mineral chemistry has avoided for too long to assess the role of the major phase making up the magma: the silicate melt. Silicate melts have been very often considered as a simple reservoir of elements almost chemically inert and fully controlled by other phases (mainly solid) able to impose their redox state, (i.e., fO_2), which in turn was treated like a Maxwell demon. However, magma is the most important transport agent throughout our planet, buffering entire planetary sectors both thermally and chemically.

This volume shows the multiple concepts and approaches useful to the study of the complex interactions occurring between melts, crystals, and fluids that are behind magma formation, ascent, and evolution. By joining the description of magma physical chemistry with geological issues, the chapters of this book disclose the multifaceted implications that redox variables and their gradients have on magma evolution in time and on the dynamics of planet Earth, or in other words, it brings to the reader's attention the power of redox geodynamics.

This volume provide a comprehensive overview and a state-of-the-art treatment of technological and scientific advances in our understanding of redox geochemistry. Given the almost infinite conditions of temperature, pressure, and chemical composition relevant to igneous petrology and volcanology, the chapters represent a selection of topics able to give a unique picture of the "redox" continuum of the Earth's interiors.

Part I is composed of chapters about oxygen fugacity in Earth's accretion and across geodynamic settings, with a focus on the redox boundaries associated with mantle melting. Part II deals with the role of redox in magma differentiation, from the magma source up to the surface throughout volcanic processes, particularly degassing. Part III gives an overview on the tools and experimental and theoretical techniques to measure the redox state in melts and glasses and estimate the role of redox state on element and isotope partitioning; the major recent advances in understanding redox mechanisms affecting multivalent elements other than iron and innovative oxybarometers are presented.

This volume is the result of the sessions "Linking the Redox State of Silicate Melts to Magmatic Processes" at the Goldschmidt Conference in Paris in 2017 and "Oxygen fugacity and redox mechanisms in high- to low-temperature geochemical processes" at the AGU Fall Meeting in San Francisco in 2019. In writing up their papers, the authors have taken into consideration the discussions had during the two sessions.

The editors wish to thank all authors for their contributions and also acknowledge the assistance of the reviewers, whose conscientious efforts helped the authors to improve the quality of the chapters in this volume. The editors also wish to thank the Institut de Physique du Globe (Université de Paris) for its support, Aline Peltier (Institut de Physique du Globe de Paris – Observatoire Volcanologique du Piton de la Fournaise) for the cover image, the Volcanology, Geochemistry and Petrology (VGP) division of the American Geophysical Union (AGU), and the Commission on Physics of Mineral (CPM) of the International Mineralogical Association (IMA).

Roberto Moretti Daniel R. Neuville

Université de Paris, Institut de Physique du Globe de Paris, France

Redox Equilibria: From Basic Concepts to the Magmatic Realm

Roberto Moretti^{1,2} and Daniel R. Neuville¹

ABSTRACT

The basic aspects of redox geochemistry are reviewed to provide a useful compendium of the redox connection between the aqueous-hydrothermal and igneous realms of Earth. The redox description of a system is intimately coupled to the knowledge of acid-base properties of the solvent in which redox exchanges take place. For magmas, and then silicate melts, approaches reporting the redox state were so far cantered around the sole concept of oxygen fugacity, fO_2 . Mastering the concept of fO_2 in experimental and observational petrology was the key to constrain the processes behind the very large range of relative oxygen fugacity observed on Earth. Although current descriptions of silicate melts and magma thermodynamic properties are mainly based on oxides or minerallike molecular components, disregarding the actual melt reactivity poses many limits in our understanding of the true chemical exchanges involving oxygen, iron and the other redox-sensitive elements. Because silicate melts, unlike aqueous solutions, lack of a full acid-base description, compositional dependencies are solved by means of empirical treatments based on oxides and their combinations. However, these can bias the interpretation of redox exchanges recorded in analyzed samples and used to identify the several processes (e.g., batch or fractional crystallization, elemental recycling, degassing, deep fluid infiltration) which characterize magma evolution and its geodynamic environment. This short compendium aims at stimulating the quest for a comprehensive and unifying picture of the acid-base and redox properties of melts from which we could extrinsic its reactivity in way similar to aqueous solutions and molten salts.

1.1. GENERAL ASPECTS AND RATIONALE

1.1.1. Oxidation Number, Electron Transfer, and Half-Reactions

Oxidation-reduction (redox) geochemistry studies those natural reactions occurring on Earth in which the transfer of electrons determines a change in the oxidation number of participating chemical species. Oxidation state (or oxidation number) measures the degree of oxidation of an atom in a substance and it is the (hypothetical) charge of an atom if all bonds to atoms of different elements were 100% ionic, with no covalent bond fraction. The oxidation state of an atom is indicated with Roman numerals, whereas Arabic numbers are used for the charge on compound (e.g., in SiO₄⁴⁻, silicon has oxidation number IV and oxygen has –II, whereas 4– is the formal charge of the whole silicate ion). Charge and oxidation number are the same for monoatomic ions. The oxidation number can be positive, negative, or zero, and it can have a

Magma Redox Geochemistry, Geophysical Monograph 266, First Edition. Edited by Roberto Moretti and Daniel R. Neuville.

© 2022 American Geophysical Union. Published 2022 by John Wiley & Sons, Inc.

DOI: 10.1002/9781119473206.ch1

¹Université de Paris, Institut de Physique du Globe de Paris, Paris, France

²Observatoire Volcanologique et Sismologique de Guadeloupe, Institut de Physique du Globe de Paris, Gourbeyre, France

fractional

fractional value as well, and although very similar, it does not correspond to valency, which is an atom property and represents the number of bonds the atom needs to become stable, i.e., to complete either duplet or octet rule.

Many redox reactions are familiar to us, such as fire and combustion, rusting, and dissolution of metals. Transition metals and main group elements (e.g., N, halogens, O, S, C) have multiple oxidation states and important redox chemistry, which affect element distribution within the geochemical shells on Earth but also through the boundaries between such shells (e.g., Moretti et al., 2020a). For instance, it is the redox state of metals and ligands that complex them, which then determines (i) their "unlocking" from pristine reservoirs (e.g. minerals in which they occur at trace level); (ii) their mobility on Earth through carriers such as magma, water, or vapor; and eventually (iii) their accumulation and precipitations in new phases making up ore deposits.

Redox reactions involve a coupled transfer of electrons, so for any oxidation (loss of electrons) a reciprocal reduction (gain of electrons) occurs. Moreover, redox reactions naturally occurring on Earth involve a net chemical change that can be described not only via the exchange of electrons between ions or their complexes, but also of oxygen and/or hydrogen atoms and compounds that these can form (e.g., Cicconi et al., 2020a and references therein). Here are some examples:

$$2Fe_{(s)} + O_{2(g)} \Leftrightarrow 2FeO_{(s)}$$
 (1.1)

$$2\text{FeO}_{(m)} + \text{H}_2\text{O}_{(g)} \Leftrightarrow \text{Fe}_2\text{O}_{3(m)} + \text{H}_{2(g)}$$
 (1.2)

$$Fe^{3+}_{(aq)} + \frac{1}{2}H_{2(g)} \Leftrightarrow Fe^{2+}_{(aq)} + H^{+}_{(aq)}$$
 (1.3)

$$4Fe^{2+}_{(aq)} + O_{2(g)} + 4H^{+}_{(aq)} \Leftrightarrow 4Fe^{3+}_{(aq)} + 2H_2O_{(aq)}$$
 (1.4)

$$SO_{2(g)} + 3H_{2(g)} \Leftrightarrow H_2S_{(g)} + 2H_2O_{(g)}$$
 (1.5)

In which the subscripts s, m, aq, and g refer to solid, melt, aqueous, and gas (including supercritical fluids) phases, respectively. In the five examples above, $O_{2(g)}$, $H_2O_{(g)}$, $Fe^{3+}_{(aq)}$, $O_{2(g)}$ and $SO_{2(g)}$ are oxidizing agents, whereas $Fe_{(s)}$, $FeO_{(l)}$, $H_{2(g)}$, $Fe^{2+}_{(aq)}$ are the reducing agents.

The word oxidation was introduced by Antoine Lavoisier (1777) and indicates the chemical mechanisms in which oxygen is consumed and added to a compound. The parallel mechanism in which some other compounds loose oxygen was called reduction. The oxidation number of reaction components in Reactions 1.1 to 1.5 shows that some elements have a greater affinity for electrons than others and that oxygen tends to appear with

oxidation number –II in its compounds (including the O²⁻ species in its ionic compounds). In contrast, hydrogen tends to appear with oxidation number I. Besides, hydrogen and oxygen atoms and their compounds in reaction are related to ligands making up the most important matrixes on Earth, such as aqueous solutions (including highly concentrated saline solution), supercritical fluids and gases, silicate melts or oxide, and silicate minerals making up rocks. Except for rocks, these matrixes are also important transport agents and thus redox carriers within Earth geochemical reservoirs and throughout their boundaries. Therefore, nearly all redox exchanges on Earth are related to chemical transfers involving hydrogen- and/or oxygen-based half-reactions such as (Cicconi et al., 2020a,b):

$$O_2 + 4e^- \Leftrightarrow 2O^{2-} \tag{1.6}$$

$$2H^{+} + 2e^{-} \Leftrightarrow H_{2} \tag{1.7}$$

that we will call henceforth oxygen and hydrogen electrodes (e.g., Cicconi et al., 2020a; Moretti, 2020) and in which the electron exchange is made explicit. For example, Reaction 1.1 can be written as the sum of Reaction 1.6 and:

$$2Fe^0 \Leftrightarrow 2Fe^{2+} + 4e^- \tag{1.8}$$

plus the formation of FeO oxides from its ions,

$$2Fe^{2+} + 2O^{2-} \Leftrightarrow 2FeO$$
 (1.9)

in which oxidation numbers and then formal charges of involved atoms do not vary.

In ore geochemistry, but also in metallurgical practice, a special mention must be made to redox mechanisms involving chalcophile elements and sulfide. Most often, relevant equilibria are written without the involvement of the medium in which they actually occur. Pyrite formation can result from the hydrothermal alteration of igneous pyrrhotite, but their equilibrium can be simply written in the sole Fe–S system as (Barton, 1970):

$$2\text{FeS} + \text{S}_2 \Leftrightarrow 2\text{FeS}_2$$
 (1.10)

In the Fe–S system, pyrite is not at the liquidus (pyrite does not melt), but as a conceptual exercise we can still relate its formation to the occurrence of the following fictitious half-reactions in the solid phase involving sulfide and polysulfide anions:

$$S_{2(g)} + 2e^- \Leftrightarrow 2S^{2-} \tag{1.11}$$

$$S_2^2 - + 2e^- \Leftrightarrow 2S^{2-}$$
 (1.12)

and their combination with iron, which appears in its cationic form Fe²⁺ in both sides of Reaction 1.10. In the

liquid state, melts in which sulfide is the main or the sole anionic ligand are very scarcely represented on Earth and segregate from reducing sulfur oversaturated magmatic silicate melts (e.g., Li and Ripley, 2013 and references therein). Instead, sulfide melts are of interest in extractive metallurgy (e.g., Sokhanwaran et al., 2016).

1.1.2. The Redox Potential in Solutions and the Ligand Role

In redox reactions a potential difference drives the transfer electrons from an anode (negative electrode) to a cathode (positive electrode): oxidation occurs at the anode and reduction occurs at the cathode. Reactions are spontaneous in the direction of $\Delta G < 0$, which is also the direction in which the potential (defined as $E_{cathode} - E_{anode}$) is positive. In a redox reaction the anode is then the half-reaction written with electrons on the right and the cathode is the halfreaction with electrons appearing on the left side.

The electric work done by a spontaneous redox reaction, like in a galvanic cell (E > 0), is the (measurable) electromotive force of the reacting systems and equals the Gibbs free energy change (e.g. Ottonello, 1997) via the Nernst equation:

$$-nFE = \Delta G = \Delta G^0 + RT ln \prod a_i = -nFE^0$$

+
$$2.303$$
RTlog $\prod a_i = -nFE^0 + 2.303$ RTlog Q_i (1.13)

with a_i the activity of the ith component participating in the redox exchange, F as the Faraday constant (96,485 Coulomb per mole), n the number of transferred electrons, and Q the activity product. In writing redox reactions, complete electrolytes are often used because the activity coefficients are measured without extra thermodynamic assumptions, but Equation 1.13 is normally used for reactions based on individual ions. To establish a potential scale for half-reactions, we keep using the convention that electrons are reported on the left-hand side of the reaction, that is, in the sense of reduction. The potentials of half-reactions can be added and subtracted, like free energies, to give an overall value for the reaction. It is also worth noting that by convention, it was decided to use a hydrogen-electrode-scale electric potential, by setting $E^0 = 0.0 \text{ V}$ for reaction 1.7 with the constituents in their standard state (e.g., Casey, 2017). This arbitrary decision implies that (i) the Gibbs energy for H⁺_(aq), the electron (e⁻), and H_{2(g)} are all 0.0 kJ/mol, and (ii) potential difference of reactions involving the hydrogen electrode (Reaction 1.7) are given by the other halfreaction completing the redox exchange.

The electrode potential values (E⁰) hold at standard conditions: by definition, standard conditions mean that any dissolved species have concentrations of 1 m, any gaseous species have partial pressures of 1 bar, and the system is 25°C. Standard potentials represent the case where no current flows and the electrode reaction is reversible. Measuring a voltage is an indication that the system is out of equilibrium. Nernstian processes are characterized by fast electron transfer and are rate-limited by the diffusion of the electron-active species into the electrolyte. The system then spontaneously approaches equilibrium because negative and positive charged species can flow in opposite directions. At equilibrium, the voltage drops to zero and the current stops, like in dead batteries. The magnitude of the cell potential, $E^0 = E^0_{\text{cathode}} - E^0_{\text{anode}}$, may be viewed as the driving force for current flow in the circuit.

The hydrogen-electrode scale electric potential so defined, E (also indicated as E_h in aqueous solutions), is a measure of the oxidation state of a system at equilibrium relative to a hydrogen electrode. E is not a constant (for given T and P) but depends on the system composition via activities of ions entering a half redox reaction. When coupled to a compositional parameter of the system related to the activity of the ligand making up the solvent of interest, such as a_H + for aqueous solutions, E can be used to establish a kind of phase diagram that shows which species (dissolved ion species, gases, or solids) will predominate among a chosen set in the system of interest (a solution) for a given temperature.

To easily understand all this, we can look at the reaction leading to the formation of liquid water:

$$2H_{2(g)} + O_{2(g)} \Leftrightarrow 2H_2O_{(ag)} \tag{1.14}$$

which is given by the sum of Reaction 1.7 (H⁺/H₂ redox couple: the anode) and the following half-reaction (the cathode):

$$O_{2(g)} + 4H^{+}_{(ag)} + 4e^{-} \Leftrightarrow 2H_{2}O_{(ag)}$$
 (1.15)

which is governed by the O₂/H₂O redox couple. The presence of protons in both Reactions 1.7 and 1.15 shows that the overall Reaction 1.14 is defined for acidic conditions (pH < 7). For neutral or basic conditions (pH \geq 7), Reaction 1.14 can be obtained from the following two half-reactions for H₂O/H₂ and O₂/OH⁻ couples, respectively:

$$2H_2O_{(aq)} + 2e^- \Leftrightarrow H_{2(g)} + 2OH^-$$
 (1.16)

$$O_{2(g)} + 2H_2O + 4e^- \Leftrightarrow 4OH^-$$
 (1.17)

Let us now deal with Reactions 1.7 and 1.15 occurring in the acidic medium (see, for example, Ottonello, 1997). The standard potential of Reaction 1.15 is $E_{16}^0 = 1.228 \text{ V}$ and refers to a standard state of water in equilibrium at $T = 25^{\circ}C$ and P = 1 bar with an atmosphere of pure O_2 . From Equation 1.13 we obtain:

$$E_{15} = 1.228 + 0.0591 \log a \text{H}^+ + 0.0148 \log a \text{O}_2$$

= 1.228 - 0.0591pH + 0.0148 \log f \text{O}_2 (1.18)

where a and f denote activity and fugacity, respectively, pH = $-\log a_{\rm H}$ + and it is considered that $aO_2 = fO_2/fO_2^0$ with $fO_2^0 = 1$ bar.

Similarly, the redox potential related to Reaction 1.7 is then:

$$E_7 = -0.0591 \text{pH} - 0.0295 \log f \text{H}_2 \tag{1.19}$$

Equations 1.18 and 1.19, which can also be derived for Reactions 1.16 and 1.17, can be used to trace E-pH diagrams (also called Pourbaix or predominance diagrams; Casey, 2017) limiting the stability field of water (Figure 1.1) and of any other systems in which E-pH relationships can be established from the reactions of intervening species (Figure 1.2). E-pH diagrams are most used for understanding the geochemical formation, corrosion and passivation, leaching and metal recovery, water treatment precipitation, and adsorption.

For the set of species of interest, E-pH diagrams show boundaries that are given by:

1. lines of negative slope that limit the stability field of water (Equations 1.18 and 1.19) or related to solid–solid phase changes in which paired electron–proton exchanges occur because the ligand (water) participates in reaction, such as in the case of the hematite–magnetite boundary in Figure 1.2:

$$3Fe_2O_3 + 2H^+ + 2e^- \Leftrightarrow 2Fe_3O_4 + H_2O$$
 (1.20)

Note that boundary slope is negative because protons and electrons appear on the same side of reaction. The protons/electrons ratio determines the slope value.

2. (rare) pH-dependent lines of positive slopes, and associated with electron-proton exchanges involving, for example, reduction of dissolved cations to the oxide with a lower oxidation number, e.g.

$$2Cu^{2+} + H_2O_{(aq)} + 2e^- \Leftrightarrow Cu_2O_{(s)} + 2H^{+-}$$
 (1.21)

Boundary slope is positive because protons and electons appear on different sides of reaction.

3. horizontal lines (pure electron exchange), such as in case of half-reaction

$$Fe^{3+} + e^{-} \Leftrightarrow Fe^{2+} \tag{1.22}$$

which participates with half-reaction 1.7 in giving Reaction 1.3 and does not involve explicitly the water solvent.

4. vertical lines, representing no change of oxidation state but only acid-base reactions (a sole exchange of protons for aqueous solutions), such as

$$2Fe^{3+} + 3H_2O \Leftrightarrow Fe_2O_{3(s)} + 6H^+$$
 (1.23)

with the boundary plotted at the pH value for which $Q_{23} = K_{23}$ with $aFe_2O_{3(5)} = (aFe^{3+})^2 = 1$ (and also $aH_2O = 1$).

We now see that Reactions 1.3 and 1.4 are both related to half-reaction 1.22, but they refer to different redox conditions and then have different meanings. In Reaction 1.3 water is the oxidizing agent in acidic conditions, whereas it is the reducing agent in Reaction 1.4 (Appelo and

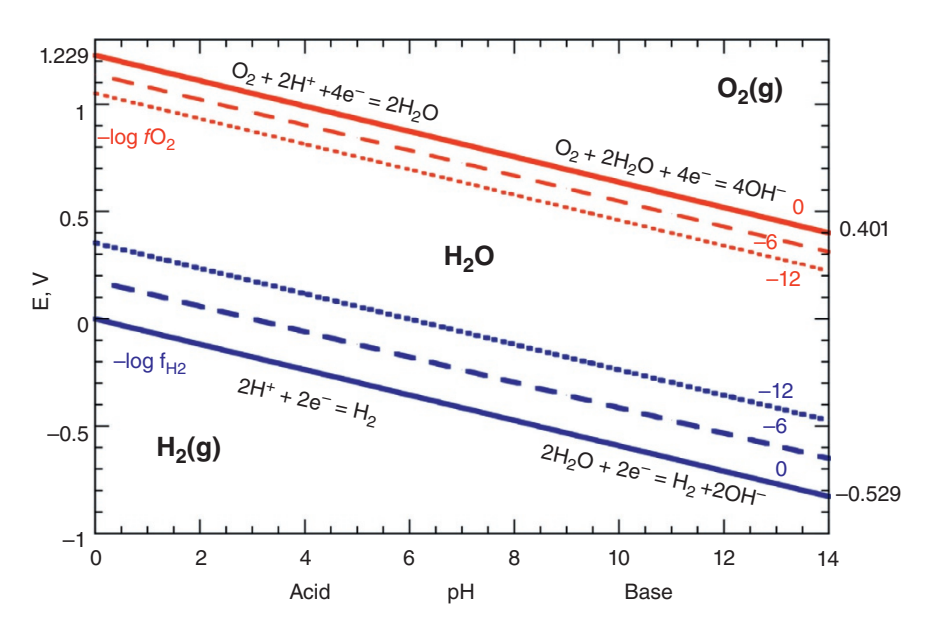


Figure 1.1 E-pH diagram reporting the stability of water at T = 25°C and P = 1 bar for different partial pressure of H_2 and O_2 (log-values).

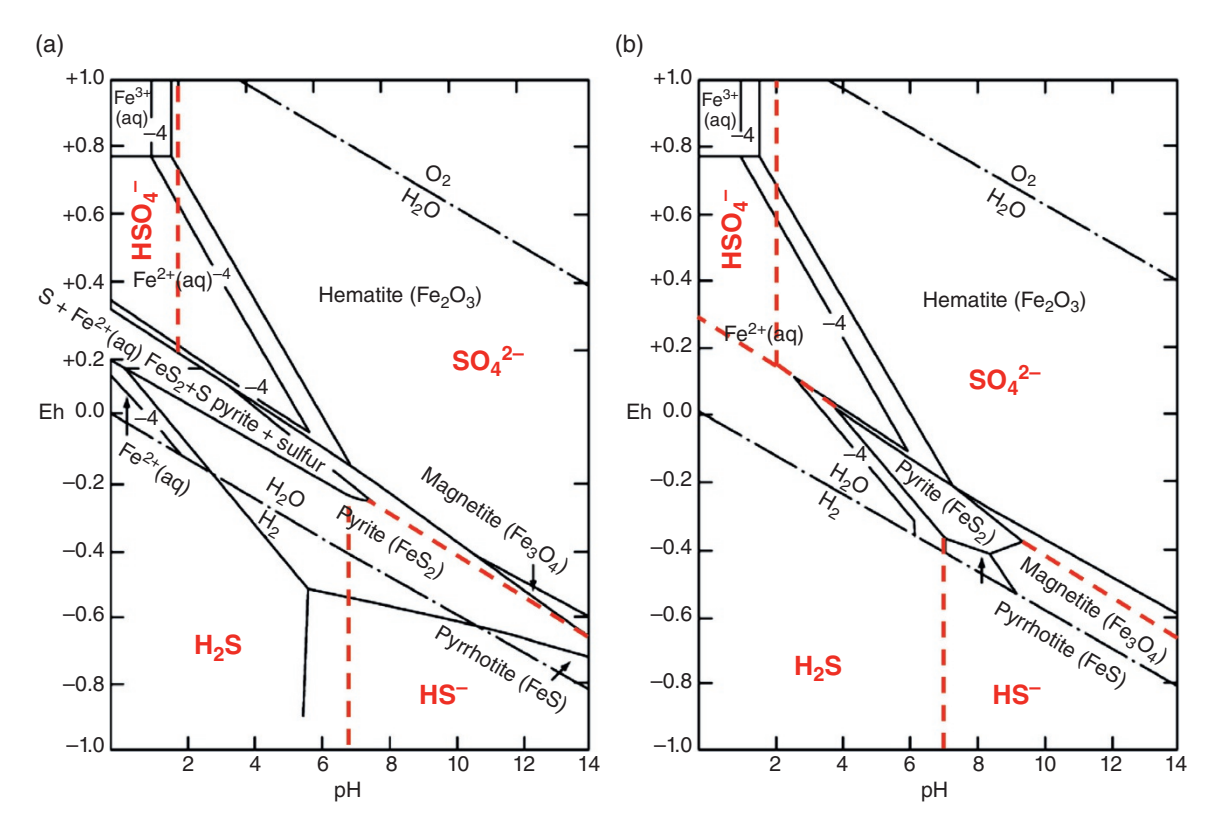


Figure 1.2 The E-pH (Pourbaix) diagram for the Fe-S-H₂O system at 25°C at 1 bar total pressure and for total dissolved sulfur activities of 0.1 (panel a) and 10⁻⁶ (panel b). Superimposed are the stability fields for H₂S, HS⁻, HSO₄²⁻ and SO₄²⁻ dissolved species (red lines, traced from data in Biernat and Robins, 1969). Note how the field of stability of pyrite, FeS2, shrinks and that of magnetite, Fe3O4, expands with decreasing total sulfur activity. Modifed from Vaughan (2005).

Postma, 1996), which represents a regulating mechanism of O₂, probably the oxidative alteration of rocks containing Fe²⁺, in particular at oceanic ridges.

Basically, E-pH diagrams demonstrate that breaking of a redox reaction into half-reactions is one of the most powerful ideas in redox chemistry, which allows relating the electron transfer to the charge transfer associated with the speciation state and the acid-base behavior of the solvent. Superimposing E-pH diagrams allows a fast recognition of the existing chemical mechanism occurring in an electrolyte medium. For example, Figure 1.2 on the Fe-H-O-S system can be seen as the result of the superposition of stability diagrams for H-O-S and Fe-O-H system. The resulting diagram in Figure 1.2 shows that the pyrite-magnetite boundary has a negative slope due to half-reaction:

$$\begin{aligned} &Fe_3O_{4(s)} + 6SO_4{}^{2-}{}_{(aq)} + 56H^{+}{}_{(aq)} + 44e^{-} \\ &\Leftrightarrow 3FeS_{2(s)} + 28H_2O_{(aq)} \end{aligned} \tag{1.24}$$

but also a positive slope well visible in Figure 1.2b due to sulfur reduction and dissolution in water as HS⁻:

$$3\text{FeS}_{2(s)} + 4\text{H}_2\text{O}_{(aq)} + 4\text{e}^- \Leftrightarrow \text{Fe}_3\text{O}_{4(s)} + 6\text{HS}^-_{(aq)} + 2\text{H}^+_{(aq)}$$
(1.25)

Reaction 1.25 implies of course a positive slope, because H⁺ appears on the right side and electrons on the left. We can also appreciate the reduction of sulfur from pyrite to pyrrhotite at pH > 7:

$$FeS_{2(s)} + H^{+} + 2e^{-} \Leftrightarrow FeS_{(s)} + HS^{-}_{(aq)}$$
 (1.26)

which has a negative slope of -0.0295pH because the number of exchanged electrons is double than protons.

These concepts can then be transferred to other solvents in which ligand-metal exchanges lead to a different speciation state and are governed by a different notion of basicity, i.e. oxobasicity, such that (see Moretti, 2020 and references therein):

Base
$$\Leftrightarrow$$
 Acid + O^{2-} (1.27)

which can be also related to redox exchanges via the normal oxygen electrode (Equation 1.6), in the same way the normal hydrogen electrode (Reaction 1.7) can be put in relation with the Bronsted-Lowry definition of acid-base behaviour in aqueous solutions (see Moretti, 2020):

Base +
$$H^+ \Leftrightarrow Acid$$
 (1.28)

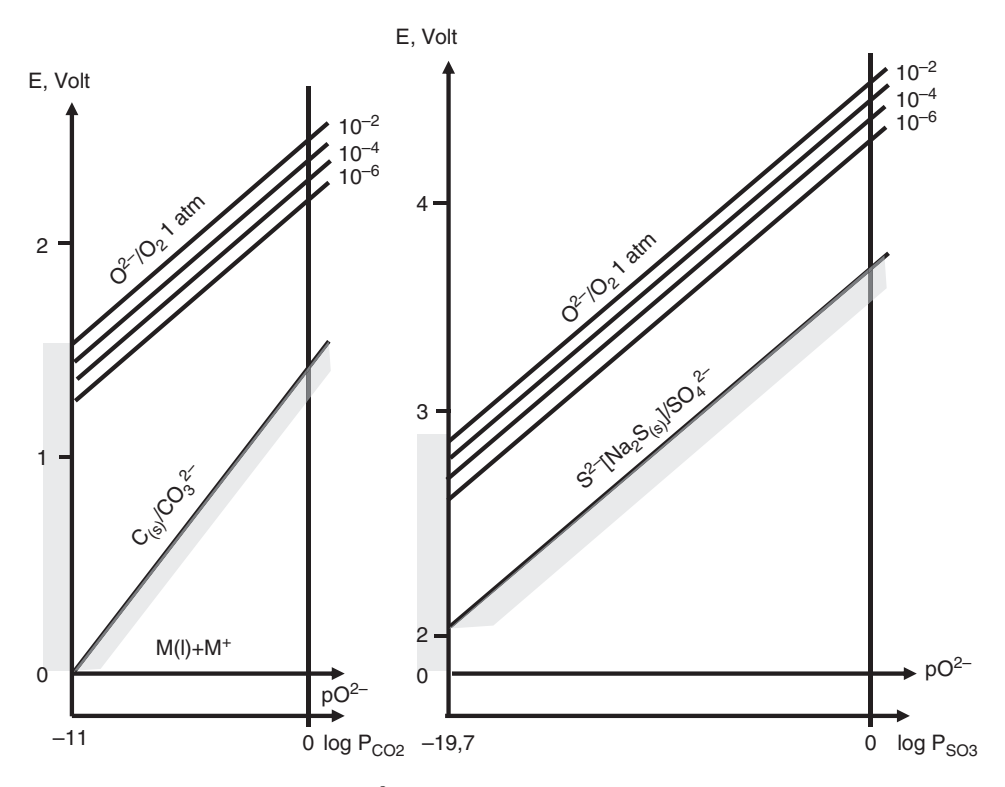


Figure 1.3 Limit of equilibrium potential-pO²⁻ graphs in molten alkali carbonates and sulfates, at 600°C (modified from Trémillon, 1974).

It is then possible to define $pO^{2-} = -log aO^{2-}$ and introduce E- pO^{2-} diagrams, in which acid species will be located at high pO^{2-} values. These diagrams were first introduced by Littlewood (1962) to present the electrochemical behaviour of molten salt systems and provide an understanding of the stability fields of the different forms taken by metals in these systems. Reference potential for molten salt is chosen either from anion or from cation, but anion, making up the ligand, is normally selected because there may be several different cations in the system.

For molten solvent diagrams, such as carbonate and sulfate melts, the stability area of the bath depends on the salt itself and can be seen by using as examples oxyanion solvents (Figure 1.3). Limitations on the pO²⁻ scale of oxoacidity (Reaction 1.27) are given by the values of the Gibbs free energy of the formation reactions of alkali carbonates or sulfates at the liquid state, which depends on temperature as well as on pressure. On the basic side (low pO²⁻ side) the limit is imposed by the solubility threshold of the generic $M^{\nu+}O_{\nu/2}$ oxide in the electrolyte medium, i.e., $pO^{2-}min \approx M^{\nu+}O_{\nu/2}$ solubility, whereas on the acidic side the limit is imposed by P_{CO2} or $P_{SO3} = 1$ bar. For example, it is 11 units in the case of the ternary eutectic Li₂CO₃+Na₂CO₃+K₂CO₃ at 600°C and 19.7 units in the case of the ternary eutectic Li₂SO₄ + Na₂SO₄ + K₂SO₄ at the same temperature (Trémillon 1974; Figure 1.3).

The upper stability limit is related to the $O^{-II}/O_{2(g)}$ redox system (Reaction 1.6), i.e., to the oxidation of CO_3^{2-} and SO_4^{2-} anions:

$$CO_3^{2-} \Leftrightarrow {}^{1}/_{2}O_{2(g)} + CO_{2(g)} + 2e^{-}$$
 (1.29)

$$2SO_4^{2-} \Leftrightarrow \frac{1}{2}O_{2(g)} + S_2O_7^{2-} + 2e^-$$
 (1.30)

which results from acid-base exchanges of the type:

$$CO_3^{2-} \Leftrightarrow CO_{2(g)} + O^{2-}$$
 (1.31)

$$2SO_4^{2-} \Leftrightarrow S_2O_7^{2-} + O^{2-}$$
 (1.32)

coupled to half-reaction 1.6.

Both Reactions 1.29 and 1.30 yield the E-pO²-relationship:

$$E = E_{O_2}^0 + \frac{2.3RT}{4F} \log P_{O_2} + \frac{2.3RT}{2F} pO^{2-}$$
 (1.33)

The lower stability limit of the solvent can be given by either the reduction of alkaline cation in the corresponding metal:

$$M^{\nu^+} + \nu e^- \Leftrightarrow M_{(1)} \tag{1.34}$$

whose potential is independent of pO^{2-} , or the reduction of CO_3^{2-} and SO_4^{2-} anions given by:

$$CO_3^{2-} + 4e^- \Leftrightarrow C_{(s)} + 3O^{2-}$$
 (1.35)

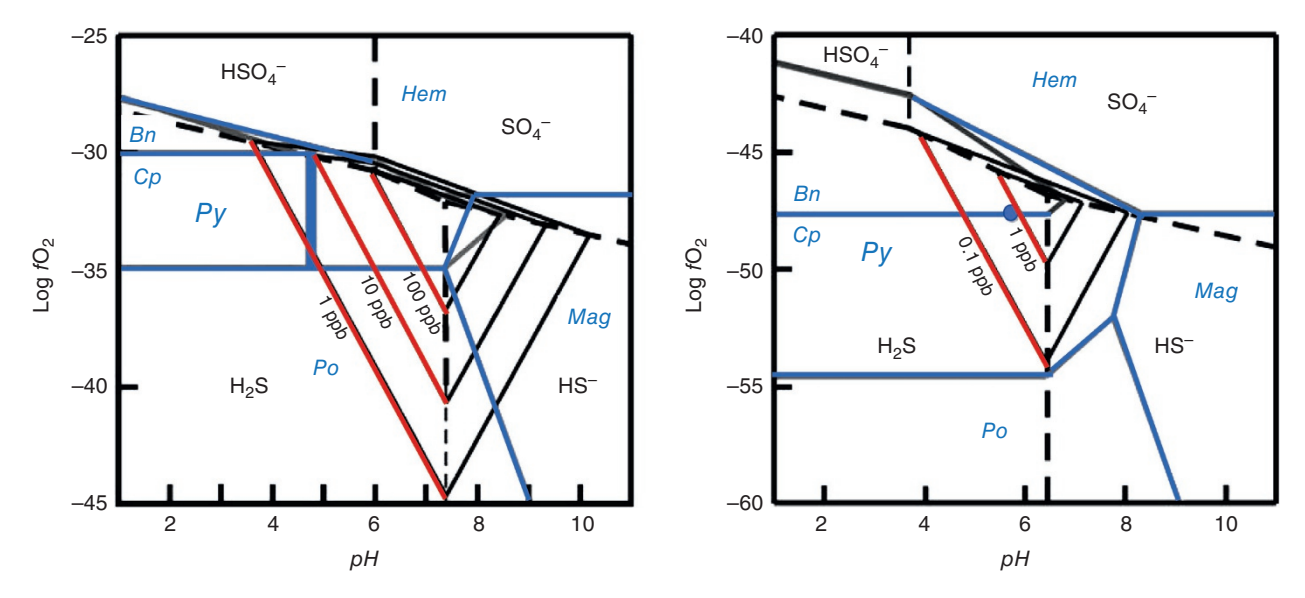


Figure 1.4 Log fO₂ - Ph diagrams for 290°C (left panel) and 145°C (right panel) at saturated vapor pressure, showing predominance fields for aqueous sulfur species (dashed lines), stability fields for Fe-O-S minerals and bornitechalcopyrite (solid grey lines). The solubility contours (left panel: 1, 10, 100 ppm; right panel: 0.1, 1 ppm) are for gold in the form Au(HS)₂⁻. Modified from Raymond et al. (2005).

$$SO_4^{2-} + 8e^- \Leftrightarrow S^{2-} + 4O^{2-}$$
 (1.36)

and to which the following E-pO $^{2-}$ relationships correspond (CO $_3$ $^{2-}$ and SO $_4$ $^{2-}$ anions having unitary activity):

$$E = E_{C/CO_3^{2^-}}^0 + \frac{3}{4} \cdot \frac{2.3RT}{F} pO^{2^-}$$
 (1.37)

$$E = E_{S^{2-} / SO_4^{2-}}^0 - \frac{2.3RT}{8F} \log [S^{2-}] + \frac{2.3RT}{2F} pO^{2-}$$
 (1.38)

Figure 1.3 shows the results on carbonate and sulfate melts (modified from Trémillon, 1974, and references therein). The utilizable regions appear as quadrilaterals on the E-pO² graph. If in sulfates, the region is a parallelogram similar to the E-pH region in aqueous solution, the theoretical range of potential in molten carbonates appears more restricted in an oxoacidic medium than in an oxobasic medium, because the lower limit varies versus pO²- with a slope greater than that of the upper limit (Trémillon, 1974).

Silicate melts have been so far an underestimated electrolytic medium acting as a solvent for oxides. This is mainly because E-pO2- diagrams cannot be based on predictive thermodynamics and physical chemistry assessments such as the dilute electrolyte concept and its developments in the case of previous solvents, aqueous solutions particularly (Allanore, 2015). In silicate melts, and more generally molten oxides, oxygen toutcourt cannot be identified as the solvent, despite its abundance. Silicate melts are in fact a high-temperature highly interconnected (polymerized) matrix in which solvation units cannot be easily defined and both ionic and covalent bonds rule the reactive entities that make

up the melt network. Because of this, some approaches have been formalized in terms of the Lewis acid-base definition (network formers and their oxides, such as SiO₂ and Al₂O₃ are acids; network modifiers and their oxides such as MgO, CaO, Na₂O are bases) by using electronegativity and optical basicity that allow distinguishing and calculating three types of oxygen (bridging, non-bridging, and so-called free oxygen) whose mixing determines the polymerization and the thermodynamic properties of the melt mixture as a function of composition (Toop and Samis, 1962a,b; Allanore, 2013, 2015 and references therein: Moretti, 2020 and references therein). Nevertheless, silicate melts still lack a fully developed acid-base framework formalizing the thermodynamic properties of reactive species formed during the solvolysis, as the solvent itself changes its polymerization properties upon introduction of other oxide components, which are highly soluble contrary to what observed for salts in aqueous solutions. The most general thermodynamic approaches postulate mineral-like molecular structures to interpolate existing data.

In molten silicates the electric charge is primarily transported by cations, whose contribution increases with concentration of network modifiers, hence basicity. The major element, oxygen in its three forms and particularly O²⁻ and O-based anionic complexes do not contribute substantially to the charge transport (Dickson and Dismukes, 1962; Dancy and Derge, 1966; Cook and Cooper, 1990, 2000; Cooper et al., 1996a,b; Magnien et al., 2006, 2008; Cochain et al., 2012, 2013; Le Losq et al. 2020). This is a striking difference when comparing silicate melts

to previously described electrolytes, particularly with the aqueous electrolytes, in which the concentration of hydroxide ions or water is always large enough to sustain high current densities (Allanore, 2013). From a practical standpoint the anode reaction producing oxygen (the inverse of Reaction 1.6) is strongly impacted by the low transport of free oxide ions, that is free oxygen, which is at very low concentration. Besides, the anode design and technical performance would greatly benefit of the precise knowledge of oxygen physical chemistry in silicate melts, which for the moment is still too limited to narrow compositional ranges that have been investigated spectroscopically (Allanore, 2015).

Nevertheless, because of their nature, silicate melts can dissolve important amounts of metals. Besides, they exhibit a large range of thermal stability, with high temperature conditions that favor fast kinetics of redox exchanges. Upper temperature limits for electrochemical applications are given by the formation of gaseous silicon monoxide or by alkali oxide thermal decomposition in alkaline systems or by high vapor pressure for Mn-bearing systems (Allanore, 2015). In terms of transport properties, silicate melts are a solvent with high viscosity, a fact that is however compensated by the high diffusivity of the metal cation (Allanore, 2013), i.e., the cathode reactant.

Many measurements have however been carried out on melts of geological interest, also fostered by the interest in silicate electrolysis to produce on site metals and particularly molecular oxygen for terraformation of extraterrestrial planets (e.g., Haskin et al., 1992). Electrochemical series were then established in binary SiO₂-MO systems (e.g., Schreiber, 1987) but also in ternary joins such as the diopside one (Semkow and Haskin 1985; Colson et al., 1990) for redox exchanges of the type:

$$4M_{'(melt)}^{m+} + 2nO^{2-} \Leftrightarrow 4M_{(melt)}^{(m-n)+} + nO_{2(gas)}$$
 (1.39)

in which half-reactions of the type

$$M_{\text{(melt)}}^{m+} + ne^- \Leftrightarrow M_{\text{(melt)}}^{(m-n)+}$$
 (1.40)

combine with Half-reaction 1.7. Nevertheless, such series do not consider the effect of the solvent, the melt and its structure, in determining the speciation state (e.g., anionic or cationic) following the definition at Reaction 1.27. The effect of the solvent also includes the amphoteric behaviour of some dissolved oxides such as Fe₂O₃ or Eu₂O₃, which can behave either as acids, yielding FeO₂⁻ (i.e., FeO_4^{5-} tetrahedral units) and EuO_2^{-} (i.e., EuO_4^{5-}) or bases, yielding Fe^{3+} and Eu^{3+} cations (Fraser, 1975; Ottonello et al., 2001; Moretti, 2005; Le Losq et al., 2020). The multiple speciation behaviours determined by pO²⁻ can be summarized by the following reaction mechanism (e.g., Moretti, 2005; Pinet et al., 2006):

$$MO_{x,melt}^{(2x-m)^{-}} \Leftrightarrow MO_{y,melt}^{(2y-m+n)^{-}} + \left(x-y-\frac{n}{2}\right)O^{2^{-}} + \frac{n}{4}O_{2} \tag{1.41}$$

Predominance and stability diagrams (e.g., E-pH, E pO^{2-} , E-log fO_2 , or log fO_2 vs. the log-fugacity of pH or other gaseous species in the system such as SO₂, CO₂) depend on the availability of good thermodynamic data and especially a well-established testament of acid-base properties of the investigated system and its solvent(s). For silicate melts and glasses, such a testament is represented by the oxobasicity scale from the Lux definition (Reaction 1.27). Electrochemical experiments should then be envisioned to complete and validate the database in order to ensure predictions about forming species and measure their activities.

1.2. OXYGEN FUGACITY: THE CENTRALITY OF AN ELUSIVE PARAMETER

Voltage E and oxygen fugacity (fO_2) are both measures of oxidation state. The relation between fO_2 and E for a given electrolytic medium can be established by the anode reaction where oxygen is produced. In the case of aqueous solutions, conversion is provided by half-reaction 1.15 and Equation 1.18. We can then replace E-pH diagrams with analogous logfO₂-pH diagrams. In this treatment, the actual speciation state of solutions is still the key to investigate the system, but half-reactions are not considered, and the equilibrium values of overall reactions are used, same as for activity plots. As for E-pH plots, boundaries will shift by varying the total amount of soluble elements in the electrolytic solution, hence the activity of dissolved ionic species or the corresponding gas fugacity (e.g. when carbonates or sulfides and sulfates are present).

Figure 1.4 shows that in logfO₂-pH diagrams phase, boundaries that in E-pH diagrams were dependent on pH only (and not on the concentration of dissolved ions) are horizontal. Moreover, a quick comparison between figures 2 (Eh-pH diagram) and 4 (logfO₂-pH diagram) also shows that on the logfO₂ vs. pH representation the pyrite-magnetite boundary, which appears only for pH > 7, maintains the positive slope. At the T conditions of Figure 1.4 this boundary is represented by the overall

$$3\text{FeS}_{2(S)} + 6\text{H}_2\text{O}_{(aq)} \Leftrightarrow \text{Fe}_3\text{O}_{4(s)} + 6\text{HS}^-_{(aq)} + 6\text{H}^+_{(aq)} + \text{O}_2$$
(1.42)

Besides, at 145°C (water saturated conditions) the pyrite-pyrrhotine boundary is defined at pH > 7 and is positive because:

$$FeS_2 + 2H_2O \Leftrightarrow FeS + 2HS^- + 2H^+ + O_2$$
 (1.43)

whereas for pH < 7 the boundary is horizontal, given by the proton-free reaction:

$$FeS_2 + H_2O_{(aq)} \Leftrightarrow FeS + H_2S_{(aq)} + \frac{1}{2}O_2$$
 (1.44)

As we have already seen, when considering hightemperature non-aqueous (oxide) systems in the inner Earth geospheres, there is no acid-base framework and anchoring fO2 or E to pH makes no sense in absence of the solvent liquid water.

To measure the chemical potential of redox exchanges in higher temperature geological systems, geoscientists turned their attention to molecular oxygen transfer among molecular components such as oxides or mineral-like macromolecular entities.

The practice between geoscientists becomes to assess criteria for fO₂ (or aO₂) estimations disconnected from the formal description of the acid-base character of magmas. In particular, techniques were established involving mineral phases coexisting in igneous rock to establish thermodynamic or empiric laws and trends from quenched glasses via indirect measurements, most often of spectroscopic nature (e.g., Neuville et al., 2020). This change of perspective reflects the obvious consideration that geoscientists deal with samples (solidified rocks) made accessible at Earth's surface and which represent the final snapshots at the end of a long thermal and chemical evolution, whose a posteriori reconstruction is the objective of the geochemical (lato sensu) investigation.

We may then say that for practical reasons geoscientists remained anchored to the original Lavoisier-like definition of oxidation occurring in combustion processes, related to the exchange of oxygen molecules. The fact that most of the chemical analyses were from techniques in which oxygen was not directly determined but allowed to give oxides has also further favored these approaches.

In this framework, a mutual exchange of knowledge has always characterized the field of geochemistry and petrology on one side and that of metal extraction in metallurgy in the other. Relations of the type

$$M^{\nu +}_{2/\nu}O_{(s/l)} \Leftrightarrow 2/\nu M_{(s/l)} + 1/2O_{2(g)}$$
 (1.45)

with v the charge (positive) of the cation of the metal M in the corresponding oxide. Reaction 1.45 is the main target of extractive metallurgy (see also Reaction 1.34), but also sketches the ensemble of processes that occurred since early Earth's evolution to segregate the metallic core.

Ellingham diagrams (Ellingham 1944; Figure 1.5) are used in metallurgy to evaluate the ease of reduction of metal oxides, as well as chlorides, sulfides, and sulfates. The diagram shows the variation of the standard Gibbs

free energy of formation, ΔG^0 , with temperature for selected oxides and is used to predict the equilibrium temperature for reactions of the type of Reaction 1.45 and particularly the oxygen fugacity under which ore will be reduced to its metal. The standard Gibbs energy change of formation of a compound (the Gibbs energy change when one mole of a compound is formed from elements at P = 1 bar) is given by:

$$\Delta G_f^0 = \Delta H_f^0 - T \Delta S_f = \left[\Delta H_{298}^0 + \int_{298}^T Cp dT \right]$$
$$- T \left[\Delta S_{298} + \int_{298}^T \frac{\Delta Cp}{T} dT \right] = A + B \times T(K) \quad (1.46)$$

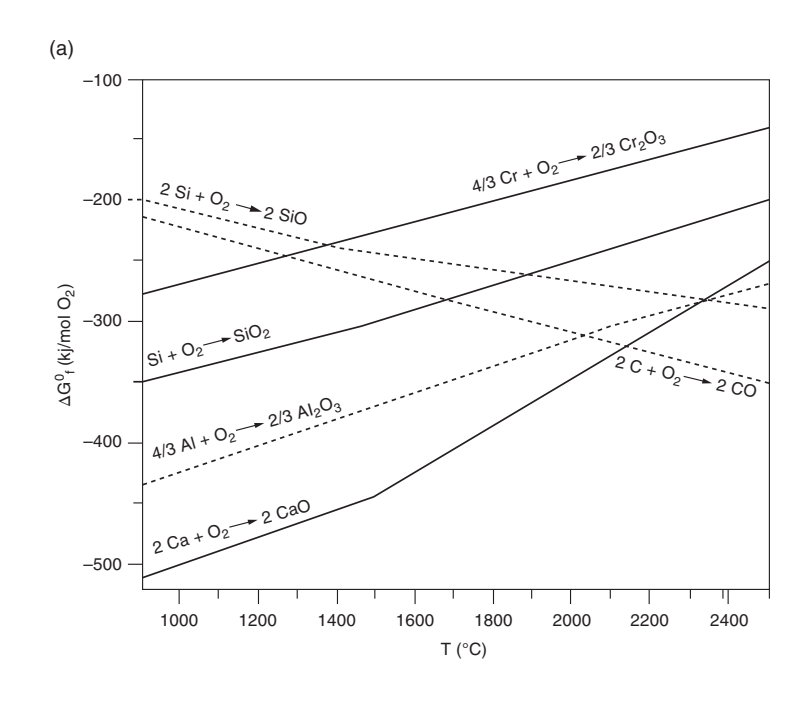
with R the universal gas constant and A and B constants.

To compare the relative stabilities of the various oxides, the Ellingham diagram is prepared for oxidation reactions involving one mole of oxygen. For the oxidation of a metal, ΔG^0 represents the chemical affinity of the metal for oxygen. When the magnitude of ΔG^0 is negative, the oxide phase is stable over the metal and oxygen gas. Furthermore, the more negative the value, the more stable the oxide is. The Ellingham diagram also indicates which element will reduce which metal oxide. The similarity between the electromotive force series (E⁰) and the Ellingham diagram, which rates the tendency of metals to oxidize, should be easily recognized.

When both Me and $Me^{\nu+}_{2/\nu}O$ in Reaction 1.45 are in their standard states, the equilibrium constant, K₄₅, corresponding to this reaction can be expressed as:

$$K_{45} = aM^{2/\nu}_{(s/l)}/aM^{\nu +}_{2/\nu}O_{(s)} \cdot 1/aO_2 = (f^0O_2/fO_2)^{1/2}$$
(1.47)

where $fO_2^{\ 0}$ is the pure gas component gas fugacity at standard state (in this case 1 bar and T of interest). If, at any temperature, the acting oxygen fugacity is greater than the calculated value from Equation 1.47, spontaneous oxidation of metal M occurs, while oxide $Me^{\nu+}_{2/\nu}O_{(s)}$ decomposes to metal Me and gaseous oxygen at the oxygen partial pressure less than the equilibrium value. In other words, an element is unstable, and its oxide is stable at higher oxygen potentials than its ΔG_f^0 -T line on the Ellingham diagram. Therefore, the larger negative value for ΔG_f^0 an oxide has, the more stable it is. In the Ellingham diagram of Figure 1.4, it can be seen, for example, that the reduction of Cr₂O₃ by carbon is possible (from the thermodynamic standpoint) at temperature above 1250°C and at each reported temperature by aluminum. It is worth noting that the Ellingham line for the formation of carbon monoxide (CO) has a negative slope, while those of all other oxides have positive slopes. As a result, at sufficiently high



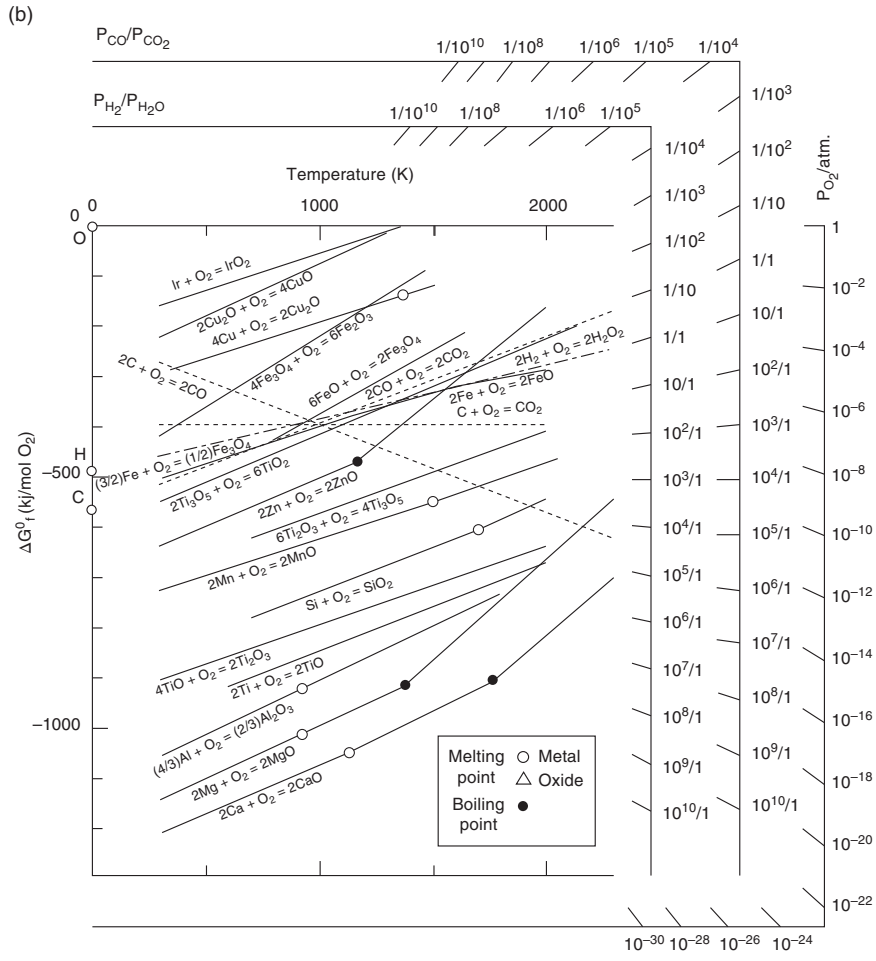


Figure 1.5 (a) Ellingham diagram for the main components of the melt/slag (solid lines) and possible reducing agents (dotted lines). The slopes of the lines representing ΔG_f^0 -T relations change at the temperature in which the phase transformations of reactants or products occur. Modified from Zhang et al. (2014). (b) Full Ellingham diagram for some relevant oxides including CO_2 equilibria and normographic scales for oxygen fugacity and related quantities via CO/CO_2 and H_2/H_2O ratios at $P_{tot} = 1$ bar. The scale of P_{H_2}/P_{H_2O} ratio is used in the same manner as that of P_{CO}/P_{CO_2} ratio, except that the point H on the ordinate at T=0 K is used instead of point C. Modified from Hasegawa (2014). All reactions' components are considered in their pure stable phase t 1 bar and T of interest.

temperatures, carbon will reduce even the most stable oxides.

Reaction 1.45 illustrates in fact how pairs of metals and their oxides, both having unitary activity, can be used as redox buffers, such that fO2 values can be easily fixed at any temperature. Even in the presence of a third phase, such as silicate melts or any other liquid, gas-solid assemblages allow a straightforward application of Equation 1.47 to impose fO2, unless solid phases are not refractory, and dissolve other components exchanges with the coexisting liquid. Reaction 1.1, involving metal iron and wustite, is a typical example (so-called IW buffer) of one of these gas-solid equilibria fixing fO_2 .

In order to illustrate the effect of the fluid phase, refined versions of the Ellingham diagrams included normographic scales, which are designed so that the equilibrium oxygen partial pressure or the corresponding P_H/P_HO or P_{CO}/P_{CO}, ratios between metal and its oxide can be read off directly at a given temperature by drawing the line connecting point O for P_O, C for P_{CO}/P_{CO}, or H for P_{H2}/P_{H2}O in Figure 1.5 and the condition of interest (Reaction 1.45 at T of interest) and then extending it to the corresponding normographic scale.

It is now quite obvious to see how both metallurgists and petrologists could then develop techniques to constrain fO₂ to investigate melting and sub-solidus conditions of oxides and silicates. After the seminal studies of Bowen and Schairer (1932, 1935) on FeO-SiO₂ and MgO-FeO-SiO₂ systems and in which the authors used iron crucibles in an inert (O₂-free) atmosphere to equilibrate the phases with metallic iron at very low but also unknown P_{O2}, early fO₂ control techniques were applied by Darken and Gurry (1945, 1946), who detailed the Fe-O system based on the use of CO and CO₂, or CO₂ and H₂, conveyed in a gas-mixer supplying a continuous mixture in definite constant volume proportions.

Later Eugster, in his early experiments to determine the phase relations of annite had to prevent its oxidation and formation of magnetite (Eugster 1957, 1959; Eugster and Wones 1962). He then developed the double capsule technique, with a Pt capsule containing the starting material, surrounded by a larger gold capsule. A metal-oxide or oxide-oxide pair plus H₂O was then placed between the two metal containers. In these experiments, reaction involving OH-bearing minerals and H₂O provides a fixed and known hydrogen fugacity (Eugster 1977), so through the dissociation Reaction 1.14 measurement of fH₂ allows calculating both fO₂ given the fH₂O at the experimental pressure $(aH_2O = 1)$ of the internal capsule.

Since Eugster, many metal-oxide and oxide-oxide assemblages have been used in experimental petrology that have been called "redox buffers." These buffers have contributed to our understanding of the role of fO2 on melt phase equilibria and mineral composition on Earth, also under volatile saturated conditions due to the possibility of evaluating fluid phase speciation at the experimental P and T conditions (e.g., Pichavant et al., 2007; Frost and McCammon, 2008. Mallmann and O'Neill, 2009; Feig et al., 2010). The results of experimental petrology made it possible to systematically collect glasses (quenched melts) to measure ratios of metals in their different oxidation states, particularly Fe^{II}/Fe^{III}, and relate such ratios to experimental P, T, and fO₂, glass composition, or other spectroscopic observations about glass/melt structure and the local coordination of targeted metals (Neuville, 2020 and references therein).

Obviously on Earth iron is the most abundant multivalent element and because of its speciation behaviour it gives rise to many reactions involving minerals and liquid (i.e., natural melts, particularly silicate ones). Reactions such as Reaction 1.1 are then useful for providing a scale with geological significance for fO₂ conditions that are recorded in rock and minerals formed in past and present Earth environments, from the core (in which Fe⁰ dominates) up to shallow crust and through all igneous environments where it exists, and Fe^{II} and Fe^{III}. To provide systematics for the aO₂ conditions the following gas-solid reactions, other than Reaction 1.1, were then assessed (Figure 1.6):

$$4Fe_{3}O_{4}+O_{2} \Leftrightarrow 6Fe_{2}O_{3} \, (magnetite-hematite; MH) \eqno(1.48)$$

$$3Fe_2SiO_4 + O_2 \Leftrightarrow 2Fe_3O_4 + 3SiO_2$$
 (fayalite – magnetite – quartz; FMQ) (1.49)

$$3\text{FeO} + \text{O}_2 \Leftrightarrow \text{Fe}_3\text{O}_4 \text{ (wustite - magnetite; WM)}$$
 (1.50)

$$SiO_2 + 2Fe + O_2 \Leftrightarrow Fe_2SiO_4 (iron - quartz - fayalite; IQF)$$

$$(1.51)$$

All these equilibria have the interesting feature of displaying unitary activities for oxide component appearing as pure phases, such that their equilibrium constants simply describe the variations of O2 activity (aO2) with temperature:

$$\log f O_2 = A/T + B \tag{1.52}$$

or, by defining fugacity, with temperature and pressure:

$$\log f O_2 = A/T + B + C(P-1)/T \tag{1.53}$$

with A, B, and C constants. The pressure term, C, allows computing directly fO_2 rather than aO_2 at the pressure of interest. Mineral assemblages making up Reactions 1.1 and 1.44 to 1.47 are not necessarily occurring in deep Earth and igneous environments, whereas the actual multi-component space of phases fix the aO_2 via multiple equilibria in which solid solutions and/or the presence of

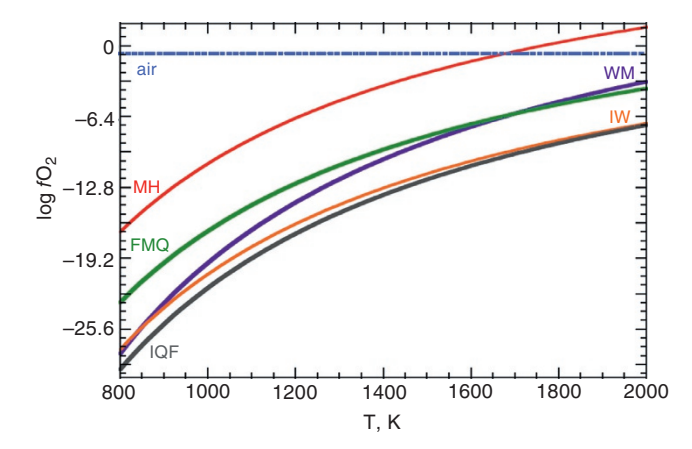


Figure 1.6 Common solid oxygen buffers used in petrology and geochemistry. The lines represent the fugacity-temperature conditions where the phases coexist stably. FMQ: fayalite, magnetite, quartz: IW: iron-wüstite: WM: wüstite-magnetite: HM magnetite-hematite. Oxygen fugacity values were computed for a total pressure of 1 bar. Also reported is the value of $log fO_2$ in air (PO₂ ~0.21 bar).

relatively mobile liquid (silicate melts) and/or supercritical fluids play a fundamental role.

However, when one of these mineral "buffers" is selected as a reference, the acting $log fO_2$ can be given as a relative value, without temperature:

$$\Delta buffer = \log f O_2 - \log f O_{2.\text{buffer}}$$
 (1.54)

A relative fO2 scale embodying temperature effects bears just a practical implication (tracking fO_2 variations with respect to a reference) but not a real meaning about logfO₂ evolution in igneous systems and related environments (e.g., Moretti and Steffansson, 2020). In particular, a common misconception was that in a system a given value of $\Delta buffer$ (e.g., $\Delta QFM = 0.5$) could represent some kind of "magic number" characteristic of the whole "rock system" throughout its thermal and chemical evolution. In natural environments oxygen activity (hence fugacity) in fact varies to accommodate the compositional variations and the speciation state of the mineral/melt/fluid phases, and also when highly mobile volatile components are involved, such that fO2 can thus be fixed by factors that are external to the system object of the thermodynamic description.

Similarly, the rock system evolution cannot be approximated by a unique Fe^{II}/Fe^{III} ratio, that the system had when completely molten. Indeed, two rocks that have ideally crystallized along the QFM buffer may have different proportions of fayalite ad magnetite because of the crystallization style but different Fe^{II}/Fe^{III} bulk ratios (Frost, 1991). However, in some systems, it is possible that the melt fixed the redox potential of the system via iron

oxidation state, with the Fe^{II}/Fe^{III} ratio approaching unity (e.g. Moretti et al., 2013).

It is also important to recall that fO_2 is just a thermodynamic parameter used to conveniently report the oxidation state of a system, particularly when O_2 is not an existing gaseous species that could be detected if the system were accessible to measurements. This is clearly proved by the very low values reported in ordinates in Figure 1.6. Therefore, fO2 turns out to be by-product of thermodynamic calculations applied to the analyses from natural samples, in which the true redox observables are the oxidation states of iron and other elements in minerals and liquids. The common practice is then to measure the concentration ratio of redox couples of multiple valence elements in melts (Fe^{II}/Fe^{III}, but also S^{-II}/S^{VI}, V^{III}/V^V, etc.) or in gases (e.g., H₂/H₂O, CO/CO₂, H₂S/SO₂) and relate them to fO₂ via thermodynamic calculations using appropriate standard state thermochemical data. As fO₂ is provided, its value is then anchored via Equation 1.54 to a given gas-solid buffer of the Reaction type 1.1 or 1.48 to 1.51. This is quite easy for gases, in which governing equilibria are directly solved if the gas analysis is provided (e.g., Giggenbach, 1980, 1987; Aiuppa et al., 2011 and references therein) and also for solid-solid equilibria, such as in case of coexisting iron-titanium oxide solid solutions titanomagnetite (Fe₃O₄-Fe₂TiO₄) and hemo-ilmenite (Fe₂O₃-FeTiO₃) (Buddington and Lindsley, 1964) or for peridotite assemblages in the mantle (e.g., Mattioli and Wood, 1988; Gudmundsson and Wood, 1995), in which the good thermodynamic characterization of solid solutions allows quite accurately treating component activities, based on mineral analyses.

On the contrary, it is much less straightforward for fO₂ estimates by oxidation states of Fe and/or S measured in glasses, as the oxybarometers derived by the study of synthetic quenched melts still suffer from too many empiric approaches. Because of their polymerized nature, silicate melts do not allow a precise distinction between solute and solvent like in aqueous solutions, where complexes and solvation shells can be easily defined in which covalence forces exhaust (see also Moretti et al., 2014). In fact, melt composition largely affects the ligand constitution and then the speciation state of redox-sensitive elements. In the case of the Fe^{II}/Fe^{III} ratio, the most common redox indicator for melts/glasses, the choice of components in reaction:

$$FeO_{(m)} + 1/4O_2 \Leftrightarrow FeO_{1.5(m)} \tag{1.55}$$

over a large compositional range (e.g., from mafic to silicic) does not offer the possibility to find accurate and internally consistent expressions for the activity coefficients of oxide components yFeO and yFeO_{1.5} (with FeO_{1.5} conveniently replacing Fe₂O₃) that solve the reaction equilibrium constant:

$$\log fO_2 = 4\log \frac{X \text{Fe}^{\text{III}}}{X \text{Fe}^{\text{II}}} + 4\log \frac{\gamma \text{FeO}_{1.5}}{\gamma \text{FeO}} + \frac{\Delta G_{1,T}^0 + \int_1^P \Delta V_{FeO_{1.5} - FeO} dP}{2.303RT}$$
(1.56)

in which the term within integral is the difference of partial molar volumes of iron components. Expansion of excess contribution to its Gibbs free energy of mixing is used to define yFeO and yFeO_{1.5} in melt mixtures. However, when these are adopted to solve Equation 1.56 for measured Fe^{II}/Fe^{III} values, they show success only over limited compositional datasets (Moretti, 2020 and references therein). Armstrong et al. (2019) calibrated volumes and interaction parameters of activity coefficients entering equation (1.56) for an andesitic melt (easily quenchable as a glass) with fO₂ buffered by the Ru-Ru₂O assemblage in the T-range 1673K to 2473K and for pressures up 23 GPa. Data fitting showed that volume term in Equation 1.56 turns from negative to positive for P > 10 GPa, which yielding iron oxidation with increasing pressure. The calibrated Equation 1.56 was then used by the authors to demonstrate how the mantle oxidized after the Earth's core started to form by a deep magma ocean with initial $Fe^{III}/Fe_{tot} = 0.04$ from which FeO disproportionated to Fe₂O₃ plus metallic iron at high temperature. The separation of Fe⁰ to the core raised the oxidation state of the upper mantle and of exsolved gases that were forming the atmosphere (Armstrong et al., 2019).

The search for one general formulation for all melt compositions of interest in petrology and geochemistry led to empirical expressions, in which adjustable parameters are introduced without the formal rigor requested by Equation 1.56 (e.g. Kress and Carmichael, 1991). These formulations furnish quite accurate fO2 values from measured Fe^{II}/Fe^{III} ratios within the compositional domain in which they have been calibrated. Besides, they often violate reaction stoichiometry and do not ensure internal consistency: if used to calculate activities they fail the application of the Gibbs-Duhem principle relating all component activities within the same phase (e.g., Lewis and Randall, 1961). Such expressions then treat fO₂ as a Maxwell's demon, doing what we need it to do to fit the calibration data and with the consequence that outside the calibration domain, all the unpredictable nonidealities are discharged on the fO₂ terms, resulting in biased calculations of fluid speciation, or other phase equilibria constraints.

As extensively treated in Moretti (2020), unpredictable non-idealities reflect counterintuitive behaviors that cannot be accounted for by activity coefficients used in the equilibrium constant of Reaction 1.55. It is well known that depending on melt composition alkali addition (i.e. decreasing pO²⁻) can either oxidize or reduce iron in the melt. This occurs because of the change of speciation

due to the amphoteric behavior of Fe^{III}, which depending on composition and then pO²⁻ can behave as either network former or modifier (see the conceptualization provided by Ottonello et al., 2001; Moretti, 2005, 2020; Le Losq et al., 2020; see also Reaction 1.41). Models that define the melt (oxo)acidity (Reaction 1.27) hence pO^{2-} (e.g. polymeric models based on the Toop and Samis mixing of bridging, non-bridging and free oxygens; see Moretti, 2020, and references therein) allows solving speciation and set activity-composition relations of ionic and molecular species, just as for aqueous solutions and molten salts.

The problem of unsolved compositional behaviors due to speciation, that are not accounted for by typical oxidebased approaches to mixtures, is exacerbated when dealing with the mutual exchanges involving iron and another redox-sensitive elements, such as sulfur. Sulfur-bearing melt species play a special role since the oxidation of sulfide to sulfate involves eight electrons: for any increment of the Fe^{III}/Fe^{II} redox ratio, there is an eight-fold increment for sulfur species (S-II/SVI; e.g., Moretti and Ottonello, 2003; Nash et al., 2019; Cicconi et al., 2020b; Moretti and Stefansson, 2020). Sulfur in magmas partitions between different phases (gas, solids such as pyrrhotite and anhydrite, and liquid as well, such as immiscible Fe-O-S liquids; Baker and Moretti, 2011 and references therein). The large electron transfer makes S^{-II}/S^{VI} a highly sensitive indicator to fO₂ changes in a narrow range (typically around QFM and NNO buffers in magmatic melts; Moretti, 2020 and references therein), whereas its effectiveness as a buffer of the redox potential is limited by the abundance of sulfur in magma, significantly lower than iron.

The modelling of joint Fe and S redox exchanges is still a major challenge which sees contrasting approaches (see Moretti, 2020). Formulations exist with various degrees of empiricism, but even those displaying better performances in exploring the $fO_2 - fS_2$ space of natural silicate melts (Moretti and Baker, 2008) should be carefully tested in reproducing phase diagrams involving multiple phases, including coexisting Fe-O-S melt, FeS_(s), and Fe₃O_{4(s)}. Introduction of sulfur equilibria in petrogenetic grids would be a major step forward for modelling in igneous petrology. Besides, it would provide the liaison with processes occurring in late- to post-magmatic stages, prior to further cooling down to real hydrothermal conditions dominated by condensed water (see Figure 1.4). For lateto post-magmatic stages, such as in the case of porphyrycopper ore formation, logfO₂-logfS₂ diagrams. Figure 7 reliably summarizes phase relations in the Fe-S-O system, in a way similar to Figure 1.2 and 1.4. It is worth noting that the diagram in Figure 1.7 can also be seen as resulting from reactivity of a sub-solidus mixed iron

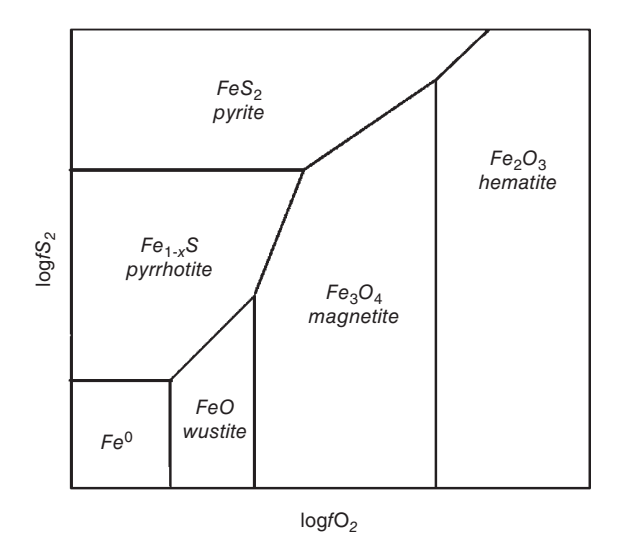


Figure 1.7 Two-redox potential fO_2 - fS_2 diagram. The conformation of stability fields in the Fe-O-S space is essentially the same also for large fO2 and fS2 variations with temperature (redrawn from Nadoll et al., 2011).

molten oxide-sulfide, in which the two main ligands are O^{2-} and S^{2-} (half-reactions 1.6, 1.11, and 1.12).

A natural assemblage of pyrite + magnetite + pyrrhotite corresponds then to the triple point marked by a star in Figure 1.7, which at a given T is invariant for fO₂ and fS₂ values given by the simultaneous occurrence of Reaction 1.10 and:

$$Fe_3O_{4(s)} + 3FeS_{2(s)} \Leftrightarrow 6FeS_{(s)} + O_2$$
 (1.57)

that allow identifying the stable phase as a function of temperature and fugacities (or activities) of reference gas species. It is worth noting that in absence of water (no H in the system represented in Figure 1.7) the boundary between FeS₂ and FeS is a function of fS₂ only (see Reaction 1.10) but not of fO_2 , as instead reported in Figure 1.4.

1.3. CONCLUDING REMARKS AND **PERSPECTIVES**

In this short compendium we show the redox features in aqueous-hydrothermal and igneous Earth. This allows the summarizing of the main redox features of a system, to show what we know of its equilibrium properties, but also what we do not know, especially for melts and magmas. We make a parallel between redox in magmas and redox in aqueous-hydrothermal solutions and show that what really changes is the way redox variables are reported. It is better described in aqueous solutions, via E-pH relations, because of the sound knowledge of acid-base

properties, which allows good prediction of system reactivity with compositional changes and fosters applications in water-based geochemistry and industrial practice (e.g. corrosion and hydrometallurgy).

Just as the measurement of pH is the key to studies of acid-base reactions, those of reactions involving the O^{2-} ion in silicate melts naturally go through the measurement of pO²⁻, a magnitude similar to pH and playing an identical role. Same as a pH indicator electrode, a pO²⁻ indicator electrode is the essential instrument to study acid-base properties of silicate melts. Technical challenges exist about this electrode as an instrument of analytical control operating directly in melts at high temperature and also as working assembly for anode reaction (inverse of Reaction 1.6). Besides, the low flux of oxide ion compared to cations is limited in melts and the lack of physical and chemical information about the molecular entities involved in the transport processes at each electrode and in the bulk of the electrolyte presents a conceptual difficulty for engineering the electrodes (Allanore et al., 2015).

Contrary to waters, in which E-pH pairs can be measured in the field by probe electrodes and then directly compared to theoretical assessments, magma-related samples do not offer the possibility to probe the conditions (temperature, pressure, gas composition, and also phase proportion) under which they equilibrated before becoming accessible to our observations. These conditions cannot be restored and must be calculated under strong assumptions, for example that glasses have preserved the same oxidation state of the melt from which they quenched. The impossibility to restore and measure the original system has surely contributed to overlooking the role played by acid-base properties and resulted in oxide-based redox descriptions of melts and magmas centred around the thermodynamic concept of fO₂, whose sole adoption was boosted by experimental petrology and the thermodynamic approach based on Ellingham's diagrams in extractive metallurgy. The acid-base concept was progressively relegated to qualitative assessments (e.g., silicic for acidic and mafic for basic).

With the exception of volcanic gases, where fO_2 (or related quantities such as fH2) can be directly measured with solid-state O₂ electrodes (Aiuppa et al., 2011 and references therein), the common practice, recently boosted by advancements in microbeam spectroscopic techniques (e.g., XANES) is to measure masses of elements in their different oxidation state and then relate such ratios to fO₂ via approaches either based on thermodynamics or having a thermodynamic flavour to solve for the role of composition. Nevertheless, such approaches are valid only in limited compositional ranges and discharges on calculated fO2 the non-ideal behaviours that are determined by speciation, hence by pO²⁻, and which cannot be reproduced by interaction parameters of oxide components (see Moretti, 2020).

These unpredictable non-ideal behaviours are reflected by the shape of the excess Gibbs free energy of mixing, which is correctly reproduced only by ionic-polymeric approaches to silicate melts mixing properties (e.g., Mao et al., 2006; Hillert et al., 1985; Ottonello and Moretti, 2004), which formalize the role of composition in establishing the relationships between polymerization and redox state in the melt. These approaches could be in perspective used to generate pO²⁻ based phase diagrams, particularly logfO₂-pO²- diagrams analogous to logfO₂-pH ones reported in Figure 1.4 for aqueous-hydrothermal solutions.

The joint description of acid-base properties and redox exchanges via predominance and stability diagrams would reduce ambiguities about the role of redox state and the "who controls what" dilemma: is fO2 a rather elusive parameter, or is it the bulk composition in the system that fixes the observed redox state? Besides, they would help in providing a more complete and formal redox description of geodynamic settings, in particular of how the redox state of magmas is a reflection of the source signature or the result of subsequent modifications due to magma evolution via partial melting, fractional crystallization, assimilation, or degassing (Carmichael, 1991; Burgisser and Scaillet, 2007; Gaillard et al., 2015; Moretti and Stefansson, 2020 and references therein) whose understanding would be beneficial at the scale of a single volcanic system to improve the forecasting of eruptions at both open-conduit (generally basaltic) and closed-conduit (generally andesitic) volcanoes via gas monitoring. Besides, this would better constrain the role of redox state on Earth's evolution since its formation and accretion.

ACKNOWLEDGMENTS

We thank Alexander Pisch (SIMAP, CNRS, France) and Maria Rita Cicconi (FAU, Germany) for their valuable reviews. The precious support of AGU Books editorial staff is greatly acknowledged. This study contributes to the IdEx Université de Paris ANR-18-IDEX-0001.

REFERENCES

- Aiuppa, A., Shinohara, H., Tamburello, G., Giudice, G., Liuzzo, M., & Moretti, R. (2011). Hydrogen in the gas plume of an open-vent volcano, Mount Etna, Italy. Journal of Geophysical Research: Solid Earth, 116(B10). https://doi.org/ 10.1029/2011JB008461
- Allanore A. (2013). Electrochemical engineering of anodic oxygen evolution in molten oxides. Electrochimica Acta, 110 (2013), 587-592.
- Allanore A. (2015). Features and challenges of molten oxide electrolytes for metal extraction. Journal of the

- Electrochemical Society, 162, E13-E22. https://doi.org/ 10.1149/2.0451501jes
- Appelo C. A. J., & Postma, D. (1996). Geochemistry, groundwater and pollution. Rotterdam: Balkema. 536 pp.
- Armstrong, K., Frost, D. J., McCammon, C. A., Rubie, D. C., & Ballaran, T. B. (2019). Deep magma ocean formation set the oxidation state of Earth's mantle. Science, 365 (6456), 903-906. doi: 10.1126/science.aax8376
- Baker, D. R., & Moretti, R. (2011). Modeling the solubility of sulfur in magmas: a 50-year old geochemical challenge. Reviews in Mineralogy and Geochemistry, 73(1), 167-213. https://doi.org/10.2138/rmg.2011.73.7
- Barton, P. B., Jr. (1970). Sulfide petrology: Mineralogical Society of America Special Paper 3, 187–198.
- Biernat R. J., & Robins, R. G. (1969). High temperature potential/ pH diagrams for the sulfur-water system. Electrochimica Acta 14, 809-820. https://doi.org/10.1016/0013-4686(69)87003-9
- Bowen, N. L., & Schairer, J. F. (1932). The system, FeO-SiO 2. American Journal of Science, 141, 177-213. https://doi.org/ 10.2475/ajs.s5-24.141.177
- Bowen, N. L., & Schairer, J. F. (1935). The system MgO-FeO-SiO 2. American Journal of Science, 170, 151-217. doi: 10.2475/ajs.s5-29.170.151
- Buddington, A. F., & Lindsley, D. H. (1964). Iron-titanium oxide minerals and synthetic equivalents. Journal of Petrology, 5, 310–357. https://doi.org/10.1093/petrology/5.2.310
- Burgisser, A., & Scaillet, B. (2007). Redox evolution of a degassing magma rising to the surface. *Nature*, 445(7124), 194–197. https://doi.org/10.1038/nature05509
- Carmichael, I. S. (1991). The redox states of basic and silicic magmas: a reflection of their source regions? Contributions to Mineralogy and Petrology, 106(2), 129-141. https://doi. org/10.1007/BF00306429
- Casey H. W. (2017). Oxidation-Reduction Reactions and EhpH (Pourbaix) Diagrams. In: W.M. White (ed.), Encyclopedia of Geochemistry, doi:10.1007/978-3-319-39193-9_21-1
- Cicconi, M. R., Moretti, R., & Neuville, D. R. (2020a). Earth's Electrodes. Elements, 16, 3, 157–160. doi: 10.2138/ gselements.16.3.157
- Cicconi, M. R., Le Losq, C., Moretti, R., & Neuville, D. R. (2020b). Magmas are the largest repositories and carriers of Earth's redox processes. Elements, 16, 3, 173-178. doi: 10.2138/gselements.16.3.173
- Colson, R. O., Haskin, L. A., & Crane, D. (1990). Electrochemistry of cations in diopsidic melt: Determining diffusion rates and redox potentials from voltammetric curves. Geochimica et Cosmochimica Acta, 54, 3353-3367. https://doi.org/10.1016/ 0016-7037(90)90290-2
- Cochain B., Neuville D. R., Henderson G. S., McCammon C., Pinet O., & Richet, P. (2012). Iron content, redox state and structure of sodium borosilicate glasses: A Raman, Mössbauer and boron K-edge XANES spectroscopy study. Journal of the American Ceramics Society, 94, 1-12. https://doi.org/ 10.1111/j.1551-2916.2011.05020.x
- Cochain, B., Neuville, D. R., de Ligny, D., Malki, M., Testemale, D., Pinet O., & Richet P. (2013). Dynamics of ironbearing borosilicate melts: Effects of melt structure and composition on viscosity, electrical conductivity and kinetics of

- redox reactions. Journal of Non-Crystalline Solids, 373-374, 18-27. https://doi.org/10.1016/j.jnoncrysol.2013.04.006
- Cook, G. B., & Cooper, R. F. (2000). Iron concentration and the physical processes of dynamic oxidation in alkaline earth aluminosilicate glass. American Mineralogist, 85, 397-406. https://doi.org/10.2138/am-2000-0401
- Cook, G. B., Cooper, R. F., & Wu, T. (1990). Chemical diffusion and crystalline nucleation during oxidation of ferrous ironbearing magnesium aluminosilicate glass. Journal of Non-Crystalline Solids, 120, 207–222. https://doi.org/ 10.1016/0022-3093(90)90205-Z
- Cooper, R. F., Fanselow, J. B., & Poker, D. B. (1996a). The mechanism of oxidation of a basaltic glass: chemical diffusion of network-modifying cations. Geochimica et Cosmochimica Acta, 60(17), 3253–3265. https://doi.org/10.1016/0016-7037 (96)00160-3
- Cooper, R. F., Fanselow, J. B., Weber, J. K. R., Merkley, D. R., & Poker, D. B. (1996b). Dynamics of oxidation of a Fe2+-bearing aluminosilicate (basaltic) melt. Science, 274, 1173-1176. doi: 10.1126/science.274.5290.1173
- Darken, L., & Gurry, R. W. (1945). The system iron-oxygen. I. The wüstite field and related equilibria. Journal of the American Chemical Society, 67(8), 1398-1412. https://doi.org/ 10.1021/ia01224a050
- Darken, L., & Gurry, R. W. (1946). The system iron—oxygen. II. Equilibrium and thermodynamics of liquid oxide and other phases. Journal of the American Chemical Society, 68(5), 798-816. https://doi.org/10.1021/ja01209a030
- Dickson, W. R., & Dismukes, E. B. (1962). The electrolysis of FeO-CaO-SiO2 melts. Transactions of the Metallurgical Society of AIME, 224, 505-511.
- Dancy, E. A., & Derge, G. J. (1966). Electrical conductivity of FeOx-CaO slags. Transactions of the Metallurgical Society of AIME, 236, 1642.
- Ellingham, H. J. T. (1944). Reducibility of oxides and sulfides in metallurgical processes. Journal of the Society of Chemical Industry, 63, 125–133.
- Eugster, H. P. (1957). Heterogeneous reactions involving oxidation and reduction at high pressures and temperatures. The Journal of Chemical Physics, 26(6), 1760-1761. https://doi. org/10.1063/1.1743626
- Eugster, H. P. (1959). Reduction and oxidation in metamorphism. In: Abelson, P. H. (ed.) Researches in Geochemistry. Volume 1. New York: John Wiley & Sons, pp. 397–426.
- Eugster, H. P. (1977). Compositions and thermodynamics of metamorphic solutions. In: Fraser, D. G. (ed.) Thermodynamics in Geology. Dordrecht: D. Reidel Publishing Company, pp. 183-202.
- Eugster, H. P., & Wones, D. R. (1962). Stability relations of the ferruginous biotite, annite. Journal of Petrology, 3, 82-125. https://doi.org/10.1093/petrology/3.1.82
- Feig, S. T., Koepke, J., & Snow, J. E. (2010). Effect of oxygen fugacity and water on phase equilibria of a hydrous tholeiitic basalt. Contributions to Mineralogy and Petrology, 160, 551-568. doi:10.1007/s00410-010-0493-3
- Fraser, D. G. (1975). Activities of trace elements in silicate melts. Geochimica et Cosmochimica Acta, 39(11), 1525-1530. https:// doi.org/10.1016/0016-7037(75)90154-4

- Frost, B. R. (1991). Introduction to oxygen fugacity and its petrologic importance. Reviews in Mineralogy and Geochemistry, 25, 1–9, https://doi.org/10.1515/9781501508684-004
- Frost, D. J., & McCammon, C. A. (2008). The redox state of Earth's mantle. Annual Review of Earth and Planetary Science, 36, 389-420. https://doi.org/10.1146/annurev. earth.36.031207.124322
- Gaillard, F., Scaillet, B., Pichavant, M., & Iacono-Marziano, G. (2015). The redox geodynamics linking basalts and their mantle sources through space and time. Chemical Geology, 418, 217–233. https://doi.org/10.1016/j.chemgeo.2015.07.030
- Giggenbach, W. F. (1980). Geothermal gas equilibria. Geochimica et cosmochimica Acta, 44(12), 2021–2032. https://doi. org/10.1016/0016-7037(80)90200-8
- Giggenbach, W. F. (1987). Redox processes governing the chemistry of fumarolic gas discharges from White Island, New Zealand. Applied Geochemistry, 2(2), 143-161. https://doi.org/ 10.1016/0883-2927(87)90030-8
- Gudmundsson, G., & Wood, B. J. (1995). Experimental tests of garnet peridotite oxygen barometry. Contributions to Mineralogy and Petrology, 119(1), 56-67. https://doi.org/10.1007/ BF00310717
- Hasegawa, M. (2014) Ellingham Diagram. Treatise on Process Metallurgy, Volume 3, 507–513. http://dx.doi.org/10.1016/ B978-0-08-096986-2.00032-1
- Haskin, L. A., Colson, R. O., Lindstrom, D. J., Lewis, R. H., & Semkow, K. W. (1992, September). Electrolytic smelting of lunar rock for oxygen, iron, and silicon. In: Nasa. Johnson Space Center. The Second Conference on Lunar Bases and Space Activities of the 21st Century, Volume 2, 411–422.
- Hillert, M., Jansson, B. O., & Sundman, B. O. (1985). A twosublattice model for molten solutions with different tendency for ionization. Metallurgical Transactions A, 16(1), 261–266. https://doi.org/10.1007/BF02816052
- Kress, V. C., & Carmichael, I. S. (1991). The compressibility of silicate liquids containing Fe₂O₃ and the effect of composition, temperature, oxygen fugacity and pressure on their redox states. Contributions to Mineralogy and Petrology, 108(1-2), 82-92. https://doi.org/10.1007/BF00307328
- Lavoisier A. (1777) Mémoire sur la combustion en général, Académie des sciences, Mémoires de l'Académie Royale, Paris, 592-600.
- Le Losq, C., Moretti, R., Oppenheimer, C., & Neuville, D. R. (2020) In situ XANES study of the influence of varying temperature and oxygen fugacity on iron oxidation state and coordination in a phonolitic melt. Contributions to Mineralogy and Petrology, 175, 64-77. doi: 10.1007/s00410-020-01701-4
- Lewis, G. N., & Randall, M. (1961). Thermodynamics, 2nd Edition. Revised By Kenneth Pitzer and Leo Brewer. McGraw-Hill Book Company. 723pp.
- Ripley, E. M., & Li, C. (2013). Sulfide saturation in mafic magmas: Is external sulfur required for magmatic Ni-Cu-(PGE) ore genesis? Economic Geology, 108(1), 45-58. https://doi. org/10.2113/econgeo.108.1.45
- Littlewood, R. (1962). Diagrammatic representation of the thermodynamics of metal-fused chloride systems. Journal of the Electrochemical Society, 109, 525-534.

- Magnien, V., Neuville, D. R., Cormier, L., Roux, J., Hazemann, J-L., Pinet, O., and Richet, P. (2006). Kinetics of iron redox reactions in silicate liquids: a high-temperature X-ray absorption and Raman spectroscopy study. Journal of Nuclear Materials, 352, 190-195. https://doi.org/10.1016/j. inucmat.2006.02.053
- Magnien, V., Neuville, D. R., Cormier, L., Roux, J., Hazemann, J-L., de Ligny D., et al. (2008). Kinetics and mechanisms of iron redox reactions in silicate melts: The effects of temperature and alkali cations. Geochimica et Cosmochimica Acta, 72, 2157-2168. https://doi.org/10.1016/j.gca.2008.02.007
- Mallmann, G., & O'Neill, H. S. C. (2009). The crystal/melt partitioning of V during mantle melting as a function of oxygen fugacity compared with some other elements (Al, P, Ca, Sc, Ti, Cr, Fe, Ga, Y, Zr and Nb). Journal of Petrology, 50(9), 1765-1794. doi:10.1093/petrology/egp053
- Mao, H., Hillert, M., Selleby, M., & Sundman, B. (2006). Thermodynamic assessment of the CaO-Al₂O₃-SiO₂ system. Journal of the American Ceramic Society, 89(1), 298–308. https:// doi.org/10.1111/j.1551-2916.2005.00698.x
- Mattioli, G. S., & Wood, B. J. (1988). Magnetite activities across the MgAl₂O₄-Fe₃O₄ spinel join, with application to thermobarometric estimates of upper mantle oxygen fugacity. Contributions to Mineralogy and Petrology, 98(2), 148–162. https:// doi.org/10.1007/BF00402108
- Moretti, R. (2005). Polymerisation, basicity, oxidation state and their role in ionic modelling of silicate melts. Annals of Geophysics, 48, 4/5, 583-608. https://doi.org/10.4401/ag-3221
- Moretti, R. (2021). Ionic syntax and equilibrium approach to redox exchanges in melts: basic concepts and the case of iron and sulfur in degassing magmas. In: Moretti, R., and Neuville, D. R. (eds.) Redox Magma Geochemistry. Geophysical Monograph Series 266. American Geophysical Union.
- Moretti, R., & Baker, D. R. (2008). Modeling of the interplay of fO2 and fS2 along the FeS-Silicate Melt equilibrium. Chemical Geology, 256, 286-298. doi:10.1016/j.chemgeo.2008.06.055.
- Moretti, R., & Ottonello, G. (2003). Polymerization and disproportionation of iron and sulfur in silicate melts: insights from an optical basicity-based approach. Journal of Non-Crystalline Solids, 323, 111-119. https://doi.org/10.1016/ S0022-3093(03)00297-7
- Moretti, R., Arienzo, I., Civetta, L., Orsi, G., & Papale, P. (2013) Multiple magma degassing sources at an explosive volcano. Earth and Planetary Sciences Letters, 367, 95-104. https://doi.org/10.1016/j.epsl.2013.02.013
- Moretti, R., & Stefánsson, A. (2020). Volcanic and geothermal redox engines. Elements: An International Magazine of Mineralogy, Geochemistry, and Petrology, 16(3), 179–184. https:// doi.org/10.2138/gselements.16.3.179
- Nadoll, P., Angerer, T., Mauk, J.L., French, D., & Walshe, J. (2014). The chemistry of hydrothermal magnetite: A review. Ore Geology Reviews, 61, 1–32. https://doi.org/10.1016/j. oregeorev.2013.12.013
- Nash, W. M., Smythe, D. J., & Wood, B. J. (2019). Compositional and temperature effects on sulfur speciation and

- solubility in silicate melts. Earth and Planetary Science Letters, 507, 187–198. https://doi.org/10.1016/j.epsl.2018.12.006
- Neuville, D. R., Cicconi, M. R., & Le Losq, C. (2021). How to measure the oxidation state of multivalent elements in minerals, glasses and melts? In: Moretti, R., and Neuville, D. R. Magma Redox Geochemistry. Geophysical Monograph Series 266. American Geophysical Union.
- Ottonello, G. (1997). Principles of Geochemistry. Columbia University Press, 894 pp.
- Ottonello, G., & Moretti, R. (2004). Lux-Flood basicity of binary silicate melts. Journal of Physics and Chemistry of Solids, 65 (8–9), 1609–1614. https://doi.org/10.1016/j.jpcs.2004.01.012
- Ottonello, G., Moretti, R., Marini, L., & Zuccolini, M. V. (2001). Oxidation state of iron in silicate glasses and melts: a thermochemical model. Chemical Geology, 174(1-3), 157-179. https://doi.org/10.1016/S0009-2541(00)00314-4
- Pichavant, M., Costa, F., Burgisser, A., Scaillet, B., Martel, C., & Poussineau, S. (2007). Equilibration scales in silicic to intermediate magmas—implications for experimental studies. Journal of Petrology, 48(10), 1955–1972. https://doi.org/ 10.1093/petrology/egm045
- Pinet, O., Phalippou, J., & Di Nardo, C. (2006). Modeling the redox equilibrium of the Ce⁴⁺/Ce³⁺ couple in silicate glass by voltammetry. Journal of Non-Crystalline Solids, 352(50-51), 5382–5390. https://doi.org/10.1016/j.jnoncrysol.2006.08.034
- Raymond, J., Williams-Jones, A. E., & Clark, J. R. (2005). Mineralization associated with scale and altered rock and pipe fragments from the Berlin geothermal field, El Salvador; implications for metal transport in natural systems. Journal of Volcanology and Geothermal Research, 145, 81–96. doi: 10.1016/j.jvolgeores.2005.01.003
- Schreiber, H. D. (1987). An electrochemical series of redox couples in silicate melts: a review and applications to geochemistry. Journal of Geophysical Research: Solid Earth, 92(B9), 9225-9232. https://doi.org/10.1029/JB092iB09p09225
- Sokhanvaran, S., Lee, S.-K., Lambotte, G., & Allanore, A. (2016). Electrochemistry of molten sulfides: Copper extraction from BaS-Cu₂S. Journal of The Electrochemical Society, 163. D115-D120.
- Semkow, K. W., & Haskin, L. A. (1985). Concentrations and behavior of oxygen and oxide ion in melts of composition CaO·MgO·xSiO₂. Geochimica et Cosmochimica Acta, 49(9), 1897–1908. https://doi.org/10.1016/0016-7037(85)90084-5
- Toop, G. W., & Samis, C. S. (1962a). Some new ionic concepts of silicate slags. Canadian Metallurgical Quarterly, 1, 129-152. https://doi.org/10.1179/cmq.1962.1.2.129
- Toop, G. W., & Samis, C. S. (1962b). Activities of ions in silicate melts. Transactions of the Metallurgical Society of AIME, 224, 878-887.
- Trémillon B. (1974). Chemistry in non-aqueous solvents. Dordrecht: D. Reidel Publishing Company. 285 pp.
- Vaughan, D. J. (2005). Minerals/Sulphides. Encyclopedia of Geology. Elsevier. 574-586.
- Zhang, J., Matsuura, H., & Tsukihashi, F. (2014). Processes for Recycling. Treatise on Process Metallurgy, Volume 3, 1507-1561. http://dx.doi.org/10.1016/B978-0-08-096988-6.00036-5